The Thesis Committee for Timothy Bryce Phillips
Certifies that this is the approved version of the following thesis:

In-Situ Laser Control Method for Polymer Selective Laser Sintering (SLS)

APPROVED BY
SUPERVISING COMMITTEE:

Supervisor:

Joseph J. Beaman, Jr.

Scott Fish

In-Situ Laser Control Method for Polymer Selective Laser Sintering (SLS)

by

Timothy Bryce Phillips, B.S.M.E.

Thesis

Presented to the Faculty of the Graduate School of

The University of Texas at Austin

in Partial Fulfillment

of the Requirements

for the Degree of

Master of Science in Engineering

The University of Texas at Austin

May 2016

Acknowledgements

I would like to thank my advisors Dr. Beaman and Dr. Fish for giving me the opportunity to work with them. They have been endless sources of inspiration and knowledge, without which none of this would have been possible. They have given me the freedom to explore my research interests, while still guiding me through my academic endeavors.

I would like to thank all my lab mates and colleagues, past and present, who made this work possible. In particular, Walker Wroe, Austin McElroy, Samantha Taylor, and Adam Lewis. Their support and countless hours spent building our machine and running tests have brought us to where we are today.

Abstract

In-Situ Laser Control Method for Polymer Selective Laser Sintering (SLS)

Timothy Bryce Phillips, M.S.E.

The University of Texas at Austin, 2016

Supervisor: Joseph J. Beaman, Jr.

This thesis investigates thermal issues of the Selective Laser Sintering process. A method for controlling laser energy deposition in order to normalize post-sintering temperatures is presented. Infrared sensors are used to provide feedback for in-situ control of laser power with the goal of reducing the influence the pre-sintering thermal profile has on the post-sintering temperatures. By actively controlling the laser during its scanning, the post-sintering temperatures can be more accurately controlled, resulting in mechanical and geometric improvements in part quality.

Table of Contents

List of Figures

Chapter 1: Overview of Selective Laser Sintering

Selective Laser Sintering (SLS) is an additive manufacturing process that was developed at the University of Texas, Austin in the 1980's (Lou, 2012). It is a layer-based process that uses a high-powered laser to fuse a thin layer of powder together to form a cross-section of the desired part geometry. The final part is a product of stacking successive cross sections and fusing each layer to the previous layer. This paper will focus on Nylon 12 (ALM PA 650) as the powder material.

To create a part in an SLS machine, the designer first creates a 3D CAD model and feeds that into a slicing program. This slicer turns the 3D model into a stack of 2D geometries, each one 0.003-0.005 inches thick. These 2D geometries are what the SLS machine will sinter. To begin building the part, the machine is loaded with powder and a counter-rotating roller spreads thin layers of powder over the build surface. Radiative and conductive heaters are used to heat the powder temperature to just below the melting point of the material. Once the temperature has stabilized, the laser begins fusing the powder in the geometry dictated by the first 2D cross section. A new layer of powder is spread on top of the newly-fused powder and the geometry of the next 2D cross-section is sintered. This process is repeated until the entire part has been sintered and is detailed in Figure 1.

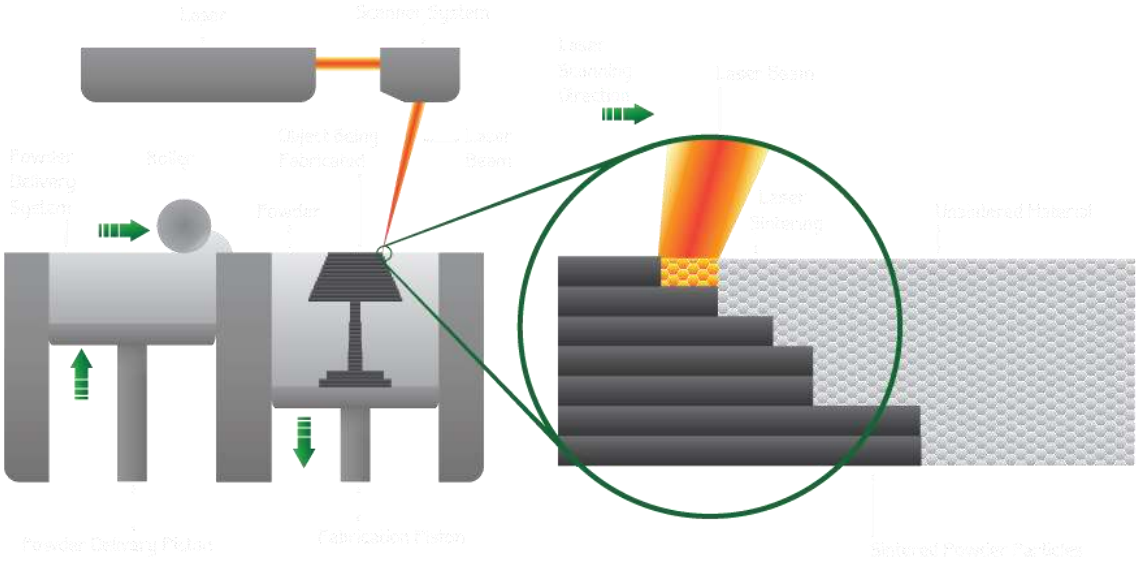

Figure 1: Selective Laser Sintering Process (Carpenter, 2014)

Chapter 2: LAMPS Experimental Machine

The LAMPS (Laser Additive Manufacturing Pilot System) was designed and built at the University of Texas, Austin as an experimental testbed and is seen in Figure 2. The specifics of this machine are well documented in other papers (Wroe, 2015), so this section will give a brief overview of the machine and highlight some of the features relevant for this experiment.

Machine Overview

The LAMPS machine has a build surface of 220 mm x 220 mm and sinters using a 60 watt CO_2 laser with a Cambridge Technologies EC1000 laser and galvanometer controller. The atmosphere is nitrogen and the temperature is controlled via strip heaters placed throughout the walls of the machine. These heaters each have a thermocouple attached to them and are regulated through a PID controller housed on a National Instruments cRIO. These heaters do the bulk of the heating for LAMPS and bring the temperature of the powder surface to just below the desired temperature. The fine tuning of temperatures is done with 3 quartz lamps. These are controlled via a FLIR A325 Long Wave Infrared (LWIR) camera that views the build surface and serves as the feedback for the quartz lamps PID loop. The view of this camera is seen in Figure 3. In addition to the strip heater thermocouples and the A325, the machine contains ambient thermocouples, a visible camera (seen in Figure 4), and a FLIR SC8240 MWIR camera, which is detailed in the next section.

Figure 2: LAMPS Machine CAD

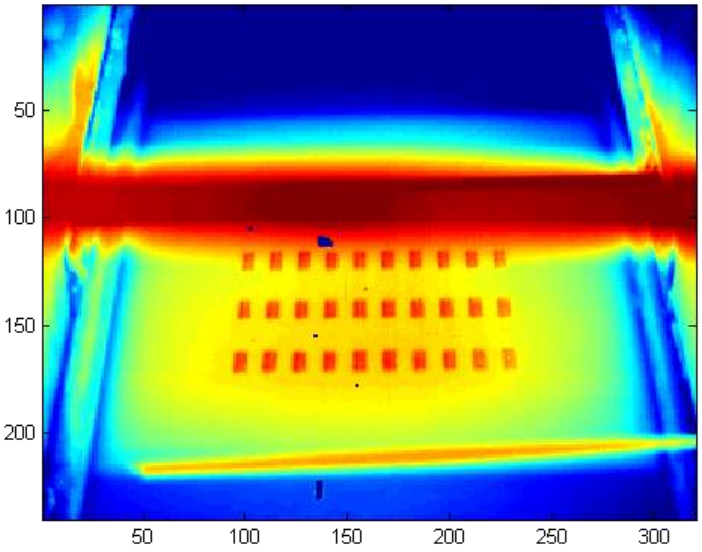

Figure 3: FLIR A325 View

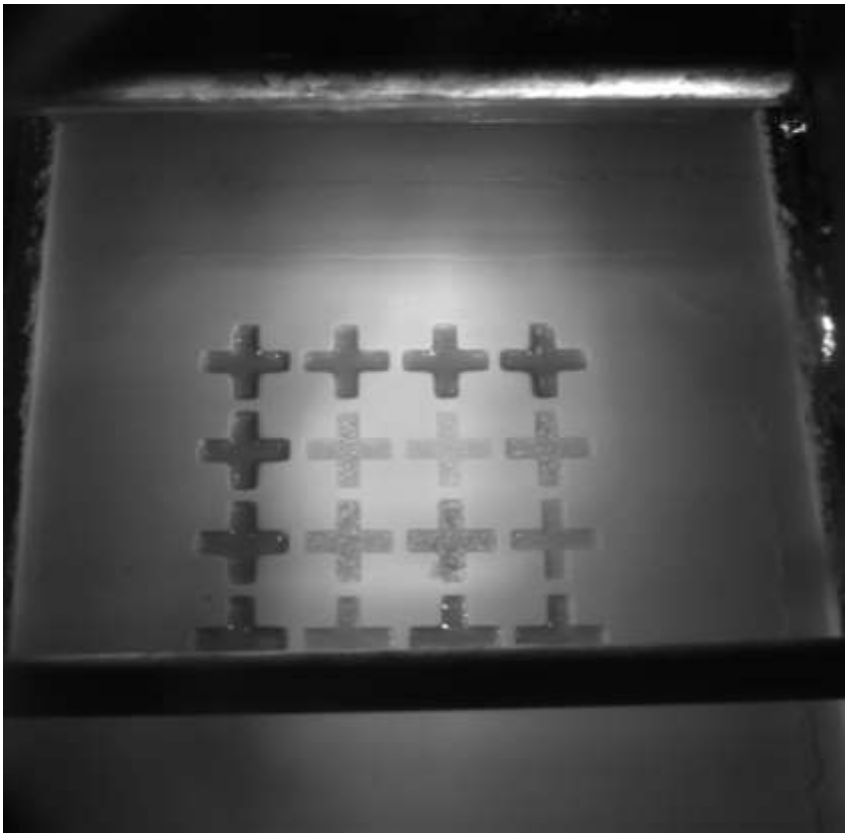

Figure 4: Visible Camera View

Boresight Camera

The FLIR SC8240 camera is a high-speed, Mid Wave Infrared (MWIR) camera capable of recording at 2,243 frames per second at 64x64 pixels. The camera is mounted in the laser box of the LAMPS machine and is boresighted with the laser beam, prior to going into the galvanometer system. By co-aligning the laser and field of view of the MWIR camera prior to the path entering the scanning system, the resulting image from the MWIR camera is a close up view of the powder surface with the laser spot fixed near the center of the image, regardless of spot position in the build chamber. The co-aligning is accomplished using a dichroic mirror that allows the CO_2 laser to pass through unobstructed and reflects the MWIR radiation into the camera. The setup is shown in Figure 5 and Figure 6.

The motivation for using a MWIR camera, as opposed to a LWIR is due to the wavelength of the CO_2 laser. The CO_2 laser, at 10.6 µm, sits in the LWIR spectrum, defined as 8-14 µm (Akhloufi, 2013). Sensors in this range will measure the radiation emitted by the powder as well as reflection of the laser, making powder temperature measurements difficult. Along with recording inaccurate temperature measurements, this can damage the camera by sending too much radiation to the camera sensor, causing pixels to burn out. The MWIR spectrum is 3-5 µm, meaning the MWIR camera will pick up the radiation in this band emitted from the powder as it is heated, while not measuring the longer wavelength laser reflection. This allows for accurate readings of the powder currently being sintered with the laser.

The MWIR boresighted camera enables sensing not seen before in polymer SLS machines. The camera's IR spectrum and framerate allow for precise measurements of laser-polymer interaction. An example of the data recorded by the MWIR camera is shown in Figure 7. This figure shows a sub-optimal velocity compensation tuning, something unable to be precisely measured previously. Velocity compensation is a tuning parameter available on the EC1000 control board that controls laser power to compensate for changes in galvanometer velocity. The galvanometers have a finite mass and are incapable of changing velocity instantaneously, meaning the beginning and end of vectors have an acceleration period. If the laser power is set to a constant value during the acceleration period, more energy is deposited in these end of vectors and the powder is heated more than the rest of the line. This phenomenon is known as end of vector over-sintering and can cause a build to be unsuccessful.

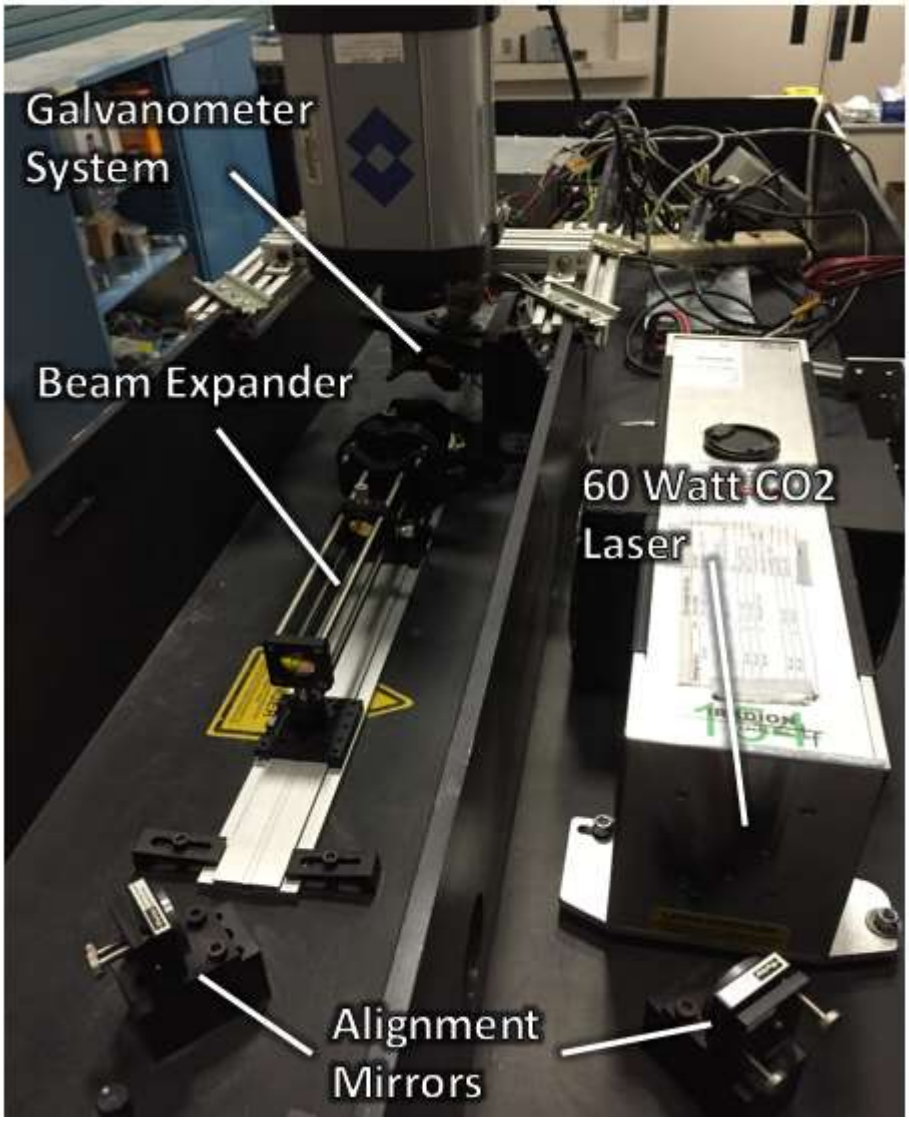

Figure 5: LAMPS Laser Box

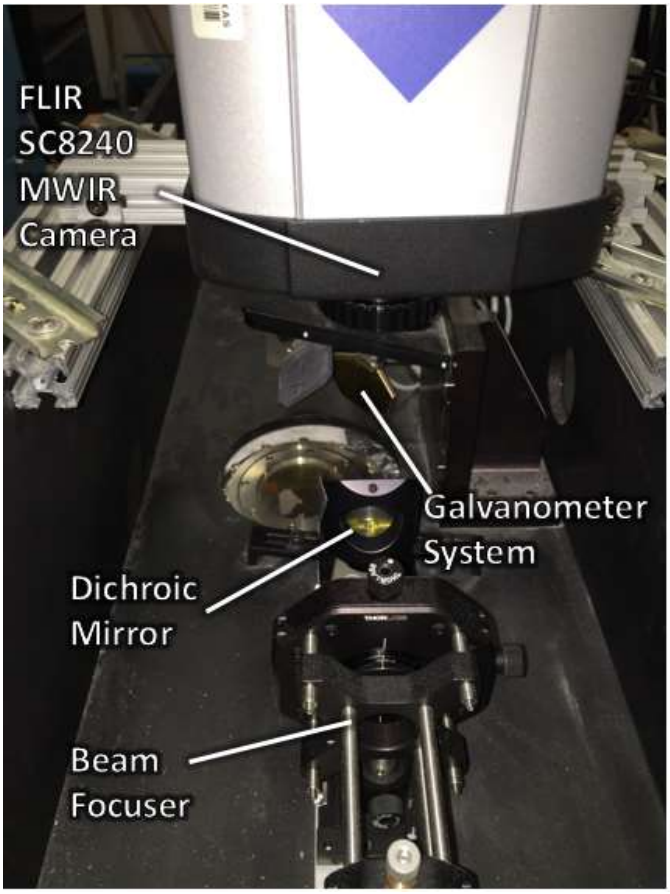

Figure 6: Dichroic Boresighting

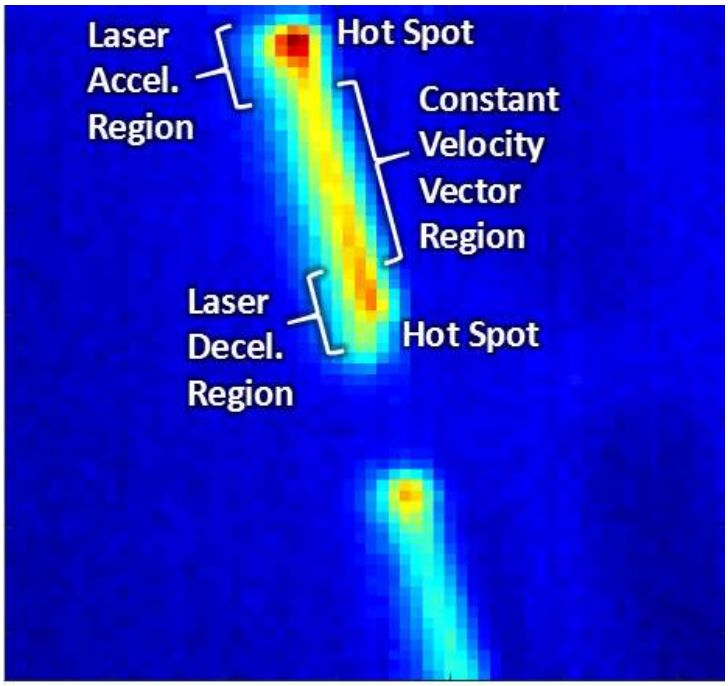

Figure 7: MWIR Camera View

Chapter 3: Experiment Motivation

Selective Laser Sintering relies on lasers to deposit patterned energy on a powder surface, raising the temperature of said surface above its melting point. A typical process control goal is to use heaters to bring the powder surface within a few degrees of the melting temperature, then use as little laser power as necessary to fully melt the powder. This process is sensitive to thermal gradients and inadequate thermal control leads to poor parts, both structurally and dimensionally. If too little energy is deposited, the material may not fully melt, leading to a structurally weak part. If too much energy is deposited, a phenomenon known as part growth may occur where the powder melts beyond the desired bounds. A third condition exists where temperature gradients cause expansion and contraction between adjacent areas of powder, curling the part (Benda, 1994).

Process-Controlled Thermal Profile

The majority of commercial SLS machines rely on resistive heaters to bring the powder surface up to temperature. Due to design constraints that limit the position of the heaters, the powder temperature can vary 10-15º C across the build surface (Hall, 2015), (Bourell, Watt, Leigh, & Fulcher, 2014). An infrared image of the powder surface in a commercial machine is shown in Figure 8. One company has retrofitted some older SLS machines with Quartz lamps to decrease the temperature non-uniformity across the powder surface (Bourell, Watt, Leigh, & Fulcher, 2014), but this still results in a gradient of ~8ºC (Hall, 2015). Further advancements have been made at University of Texas (Wroe, 2015), but there is still a gradient that must be overcome.

The CO_2 laser enters the machine through a specially-coated ZnSe lens on the top of the chamber. This lens typically has a transmission of ~95% for CO_2 wavelength (Zinc Selenide (ZnSe) Windows, 2016), but this transmission percent can change during a build. During the SLS

process, Nylon 12 will off-gas and the "fog" created can contaminate the lens (Bourell, Watt, Leigh, & Fulcher, 2014). This is not easily quantifiable as it does not affect the entire window uniformly and the transmission may drop more in some regions than others. Common practice is to clean, and sometimes polish, the lens prior to each build, but only so much of the "fog" can be removed. This "fogging" effect can decrease the transmitted laser power by up to 20-25% (Bourell, Watt, Leigh, & Fulcher, 2014), and lead to uneven temperature profiles across the powder surface as the laser power is attenuated.

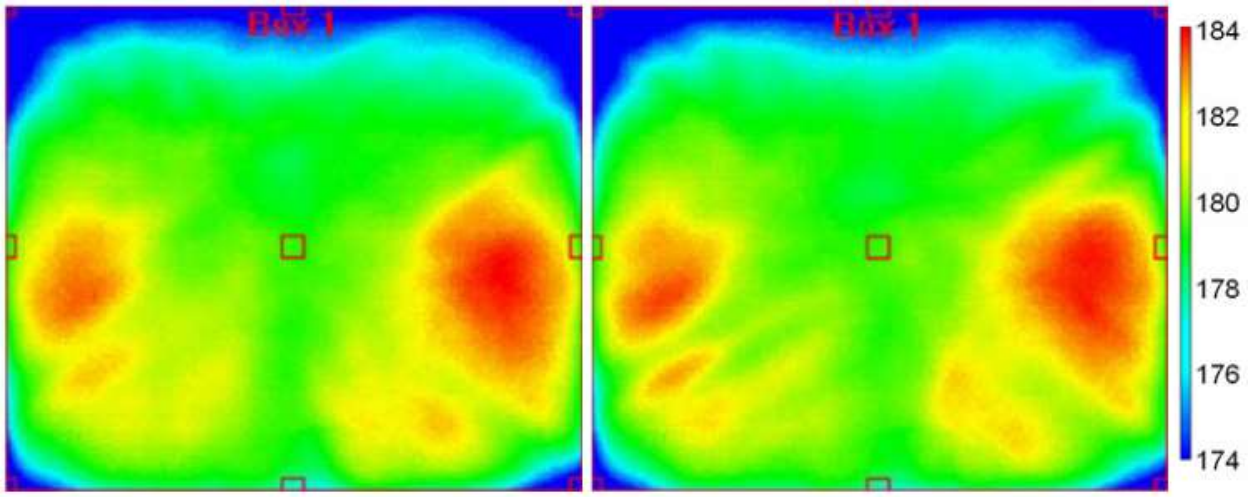

Figure 8: SLS Machine Temperature Gradient (Bourell, Watt, Leigh, & Fulcher, 2014)

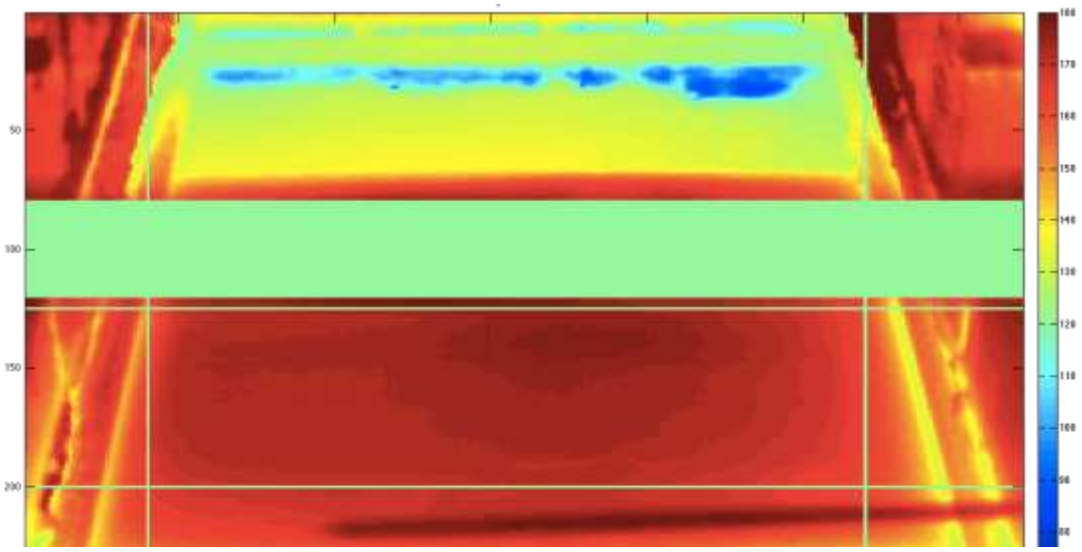

Figure 9: LAMPS Temperature Gradient (Wroe, 2015)

Build-Controlled Thermal Profile

The geometry of the part being sintered and the way the galvanometers scan the layers can cause thermal features that can also affect the localized temperatures of powder surface. The ALM PA650 powder is a good thermal insulator, but heat can still dissipate between layers and radiate away, particularly in regions where previous layers have melted powder. If a large volume of powder has been sintered in a certain region, the temperature of the new powder spread on top of that region can be affected. This is particularly prevalent when creating features such as overhangs, where a laser scan line can go from a section of powder with no sintering underneath to a section on top of an already sintered region.

The scan style of the galvanometers also contributes to the thermal profile of the powder. The most basic scanning pattern consists of scanning parallel, straight lines that overlap along their axis to ensure no un-sintered regions exist between lines. This results in a sintered region that is cooler on the first few scan lines than the bulk of the region. This is due to the first few scan lines having less overlap with already sintered powder. This can be seen in Figure 10, where the first 3

scan lines are cooler than the remaining 8. This figure shows the thermal data for one layer containing 3 tensile specimens. Each vector scan line corresponds to one of the parallel laser scan lines, where 11 lines make up the entirety of each part. More advanced scan patterns exist where the laser would sinter non-contiguous regions until the entirety of the cross-section is sintered, or a cross-hatch pattern where scan lines overlap (Scanning patterns in SLM, 2015).

The environmental conditions also effect build quality and parameters such as temperature, humidity (Kruth, Levy, Schindel, Craeghs, & Yasa, 2008), oxygen levels, etc. can influence the part by affecting powder flowability, ability to maintain temperature, and sinterability of the powder. In an open-loop system, changes in these parameters are unaccounted for, while a closed-loop control system is able to compensate for changes.

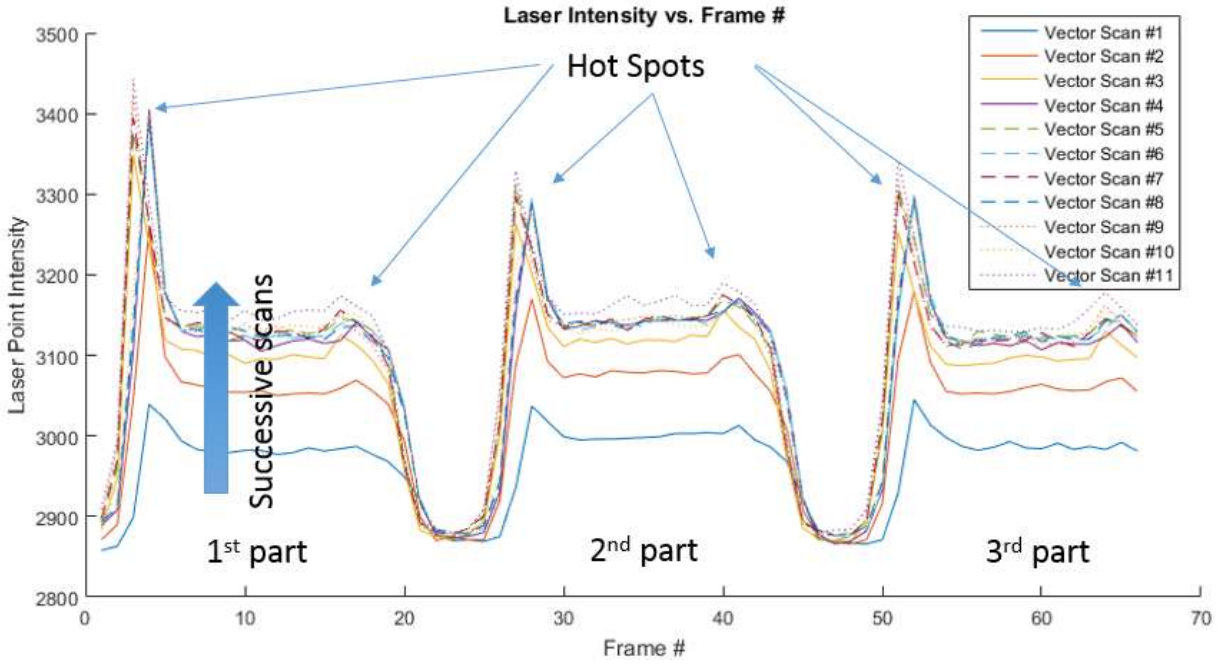

Figure 10: Scan Line Temperature

In-Situ Laser Control

In theory, a complete model of the machine and powder could be used for predictive control to change build parameters, but this is not reasonable to do in practice. SLS is a highly dynamic process and is influenced by a wide range of environmental conditions and build parameters, some still unknown. Therefore, in-situ, feedback-based laser control is a more appropriate method for achieving an even post-sintering temperature. The following sections will cover the procedure for developing and testing an in-situ control method as well as results from initial testing.

Chapter 4: Experimental Methods

An in-situ laser control procedure has been developed and tested using the LAMPS system. This chapter will discuss some hardware and software limitations and will detail the theory and practice of in-situ laser control. Many of the figures in this section use the temperature unit of counts. This unit is proportional to the energy recorded by the IR camera and is the unit exported by the FLIR SC8240 MWIR camera. It is possible to convert this unit to Celsius, but is dependent on the properties of the optical track and object being measured. These properties, such as transmittance of the optics, emissivity of the powder, and reflected radiation, are not precisely known for each test and can even change slightly throughout a test (Bourell, Watt, Leigh, & Fulcher, 2014). Therefore, it was decided to leave the unit as counts, but to give the reader a sense of scale, 7900 counts is roughly equal to 177 ºC and a 400 count change is equal to a change of roughly 3.8 ºC.

Limitations

In-Situ laser control requires two distinct actions: acquiring and analyzing data, and controlling laser energy deposition based on that analysis. It is theoretically possible to accomplish both these tasks simultaneously; however, our laser moves at 1,500 mm/sec with a spot size of 800 µm. This means a voxel of powder will only see the laser for tenths of a millisecond, making it impractical to perform the analysis and implement laser control before the laser has passed on with the current hardware.

The FLIR SC8240 MWIR camera offers framerates up to 2,243 Hz, one of the highest framerates in class. Accepting the Nyquist theorem suggests framerates in excess of 4,000 Hz are needed to precisely control the temperature of each voxel of powder using this simultaneous data

collection and implementation strategy (Koretsky, Nicoll, & Taylor, 2013). These limitations suggest that a multiple scan control strategy would be more practical and would provide enough time to react to the data.

Laser and galvanometer control is accomplished using a Cambridge Technologies EC1000. This controller is highly capable but does have limitations. The controller does not allow a user to vary the laser power or galvanometer speed mid-scan. This means that variable energy deposition will need to be accomplished by breaking the scan line into multiple segments and specifying different, fixed speeds or powers for each segment as an independent scan line.

Control Strategy

The proposed multiple scan strategy separates the control into two steps. During the first step, the galvanometers scan the boresighted MWIR camera and laser across the build surface as if they were sintering that layer, but with zero laser power. The MWIR camera is used to record the initial powder temperature, giving the initial temperature gradient of the powder surface where the laser is going to sinter. The temperature is analyzed and a scan strategy is developed to produce a line with a constant temperature, regardless of the initial temperature profile.

The second step is to employ the scan strategy developed in stage 1 to scan the laser over the desired line with the variable power it requires. The MWIR camera continues to record in this phase and is used to verify the scan strategy by examining the post-sintering temperature of the powder.

A second, similar strategy for multiple scans is to have the laser on at a low, fixed power during step 1 then continue to step 2 as described previously. An advantage of this method is that it deposits less energy during each scan, potentially reducing effects of thermal gradients, and it

can allow the galvanometers to move at a higher speed. A disadvantage of this strategy is that if the first, low-powered laser pass encounters a hot spot it is possible to increase its temperature above the final desired temperature and the hot spot will be propagated throughout multiple layers.

A third scan strategy is to scan the entire layer with the laser at a fixed power as is done during a normal build. Once the scan has finished, use the MWIR camera to record the post-sintering temperature of the powder bed and identify cold regions. Next, scan the laser at a lower power over only the cold regions in an attempt to bring them up to the same temperature as the rest of the powder. The advantage of this strategy is that it could potentially be faster than the other proposed strategies as it records and analyzes temperature data only once, for the entire layer, rather than for each individual scan line. A disadvantage is that all closed-loop control is lost on the first laser pass and it is possible to create a temperature profile that is unable to be repaired on the second scan.

This paper will focus on the first proposed scan strategy, as it provides the highest level of control and is less sensitive to the delayed timescale that arise from the software and hardware limitations.

Velocity Compensation

Galvanometers have a finite mass and, therefore, do not accelerate instantaneously. This will cause over sintering at the beginning and end of scan lines if not taken into account, as seen in Figure 10. This end of vector over sintering is a serious issue and can cause a build to crash. In order to get a constant energy deposition throughout a scan line, the laser needs to either ramp up in power during the acceleration phase of the galvanometer, or delay firing until the galvanometer speed has stabilized. Due to the EC1000 limitation that necessitates the scan line be split into

many subsections, it is imperative that this be tuned prior to using the in-situ laser control strategy discussed above. If the velocity compensation is not tuned correctly, each beginning and end of vector will display a temperature spike, so the in-situ control strategy of splitting a scan line into many subsections will yield a line with many, large temperature spikes throughout the scan line where the subsections meet.

In commercial SLS production environments, a sheet of Mylar is placed on the build surface and the markings of the laser are examined and used to adjust the velocity compensation parameters (Hall, 2015). This method is effective for tuning the parameters enough so that they do not crash a build, but lacks the definition required for in-situ control purposes. The boresighted MWIR camera has proven to be a useful tool for properly adjusting the velocity compensation with a high level of precision. End of vector over sintering can be clearly seen through the MWIR and parameters are adjusted until the temperature distribution in a scan line is sufficient. An example of the temperature distribution due to end of vector over sintering can be seen in Figure 11. In this figure, two scan lines are shown and both have a large temperature spike at the start of sintering and another, smaller spike at the end of sintering. Figure 12 shows a more acceptable tuning for velocity compensation. Measurements for both Figure 11 and Figure 12 were taken on the LAMPS machine.

On the other end of the spectrum, if the velocity compensation is too aggressive, the laser will take a long time to reach the desired power. This can cause cold regions at the beginning and end of vectors, where the laser power is still ramping up while the galvanometers are moving full speed. A tradeoff exists where the laser power ramps up quickly, but does not overshoot the desired level of energy deposition.

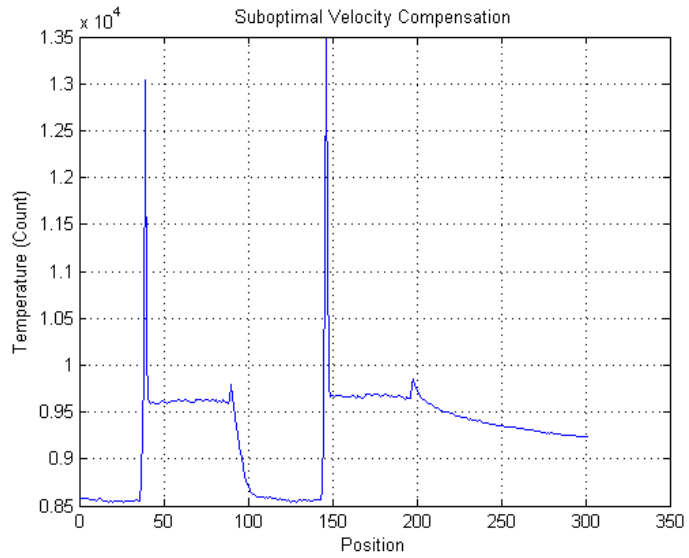

Figure 11: Suboptimal Velocity Compensation

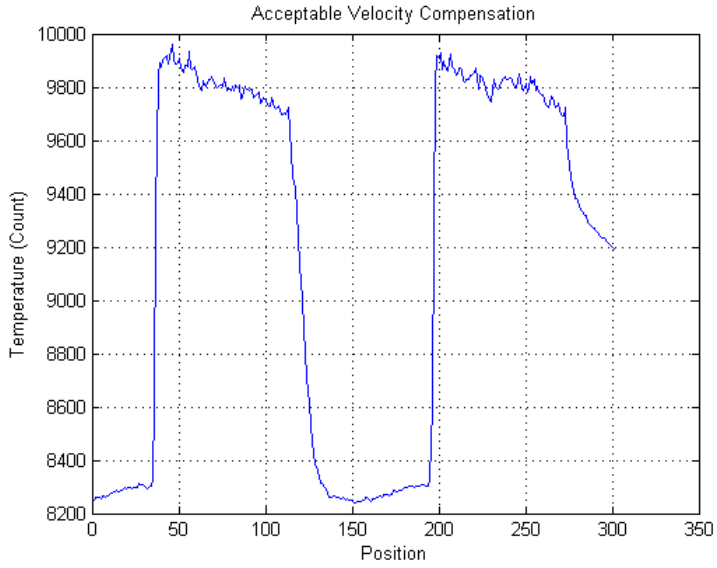

Figure 12: Acceptable Velocity Compensation

Laser Power

In order to use in-situ control of the laser power, the relationship between laser power and resulting temperature increase must be known. It is possible to build a thermal model that can predict temperature increase based on energy deposited, but that would require validation and would likely be influenced by machine parameters that are not precisely known. Therefore, for

this thesis, experimental data was used to create a laser power to powder temperature transfer function. The first step was to verify the hypothesis that a constant laser power would uniformly increase the powder temperature, preserving its original temperature gradient. Figure 13 shows the pre-sintering and post-sintering temperatures when using 10% laser power. The second subplot is the same data with the pre-sintering temperature shifted upward to coincide with the post-sintering temperature. It is clear that the post-sintering temperature mimics the pre-sintering temperature. Figure 14 shows the same data for 45% laser power and yields the same result. After more, similar tests, it is concluded that constant laser power preserves pre-sintering temperature gradients. Note that there is no large temperature spikes at end of vectors thanks to proper velocity compensation tuning.

Figure 15 shows similar data, but for a line that was split into two parts with a different power for each part. The figure shows that at both power levels, the temperature mimics the pre-sintering temperature gradient and that the only undesirable effect is a small region between the lines where the power ramps up. This region is deemed acceptable since it is so small, but further velocity compensation tuning may be able to diminish this further.

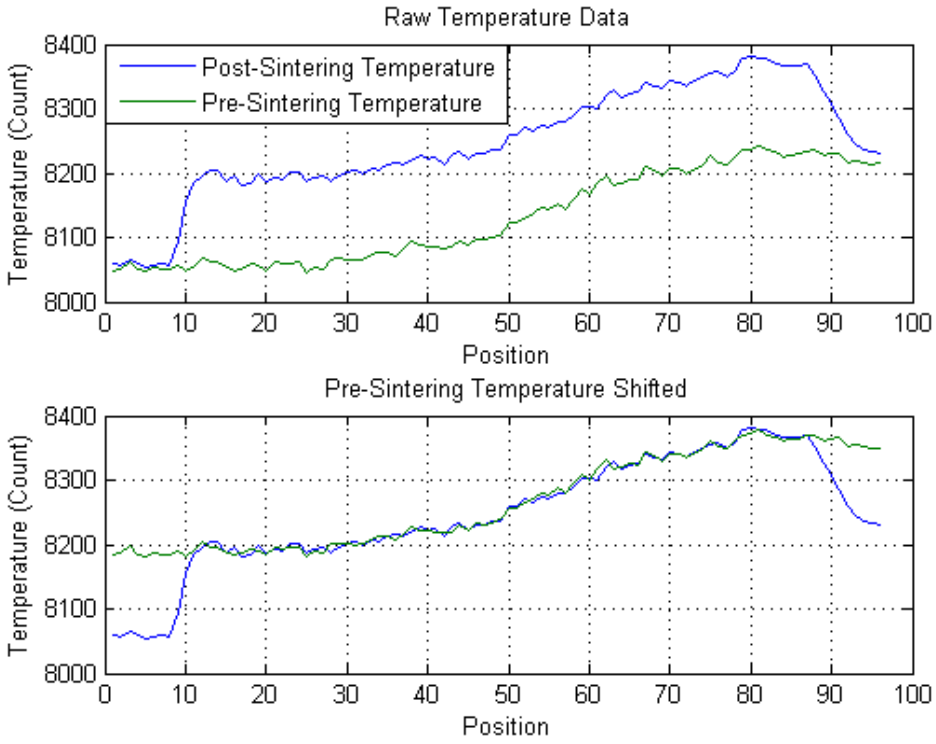

Figure 13: Temperature Comparison at 10% Power

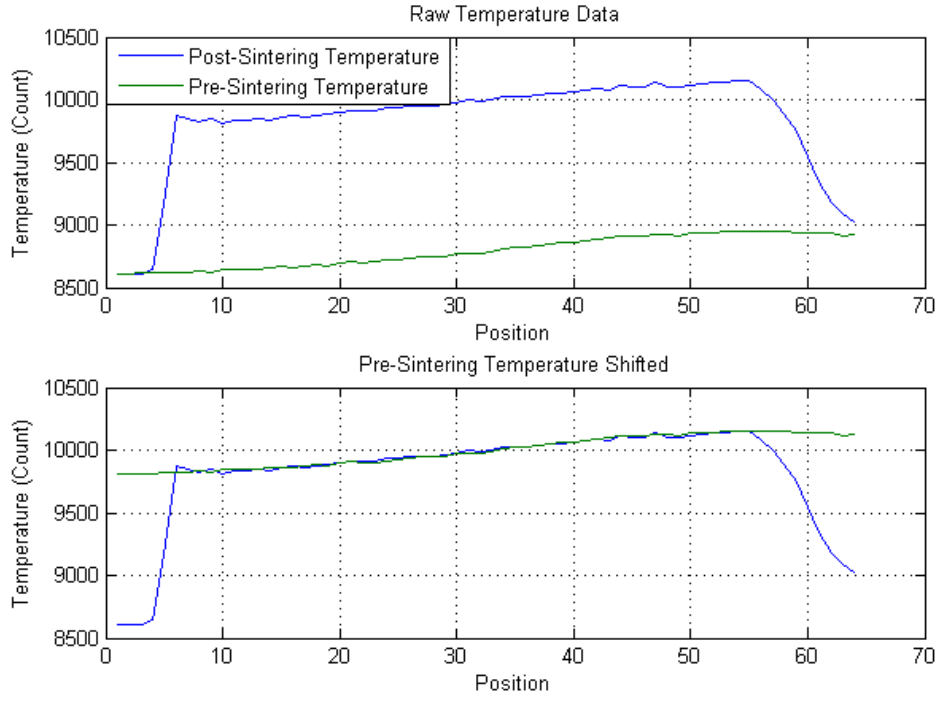

Figure 14: Temperature Comparison at 45% Power

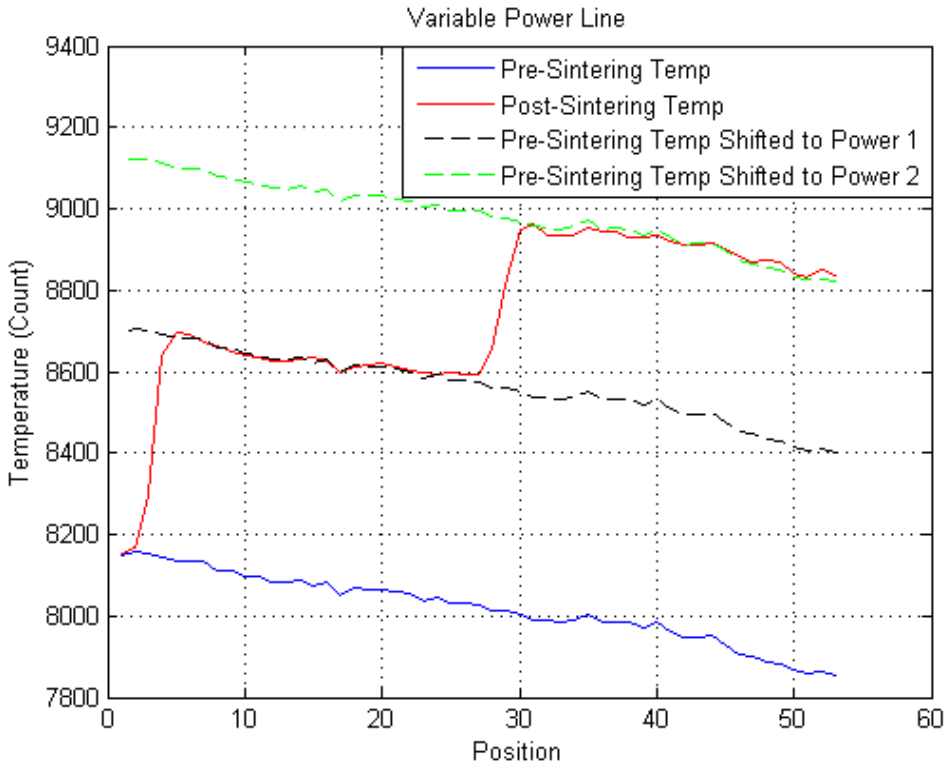

Figure 15: Temperature Comparison with Variable Laser Power

The next step was to sinter lines with different laser power percentages and compare the pre-sintering and post-sintering temperature. Powers of 5% to 50% were tested in 5% increments, with 4 test run at each power percentage. The test consisted of using the galvanometers to scan the boresighted MWIR camera over the scan line to record the initial temperature profile. Then the galvanometers scanned the same region using that test's fixed laser power. The data was analyzed and the average temperature increase for each scan line was determined. One of these trials, where laser powers of 5%, 10%, 15%, 20%, and 25% were tested is given in Figure 16. The average temperature increase for each test is shown in Figure 17, with the difference between the pre-sintering temperature and the post-sintering temperature shown on the y axis and the laser power shown on the x axis. Figure 18 shows this data with a 4^{th} order polynomial fit to the data. At 15%, 20%, and 25% laser power there was one outlier value each. These values were recorded

on the first test of those percentages and it was decided that these were questionable data points and they were to be excluded when making the laser power to temperature increase transfer function. The curve fit to the remaining data had an R^2 value of 0.9988 and was used as the laser power to temperature increase transfer function.

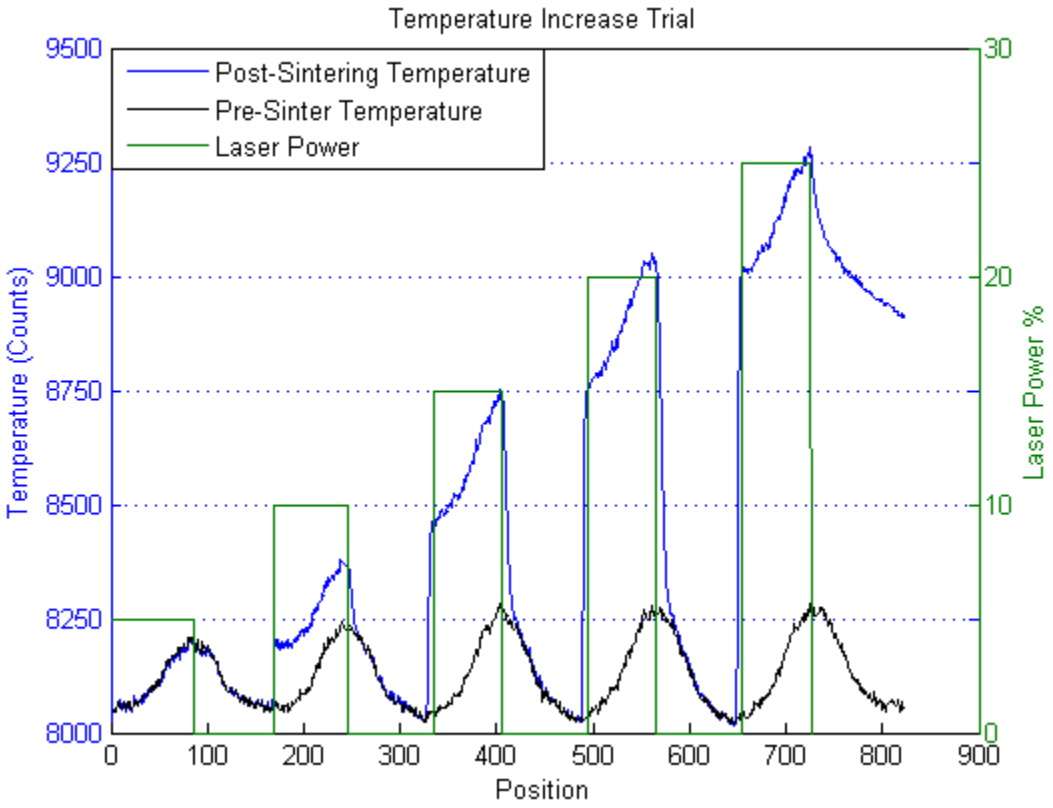

Figure 16: Laser Power and Temperature Increase Trial

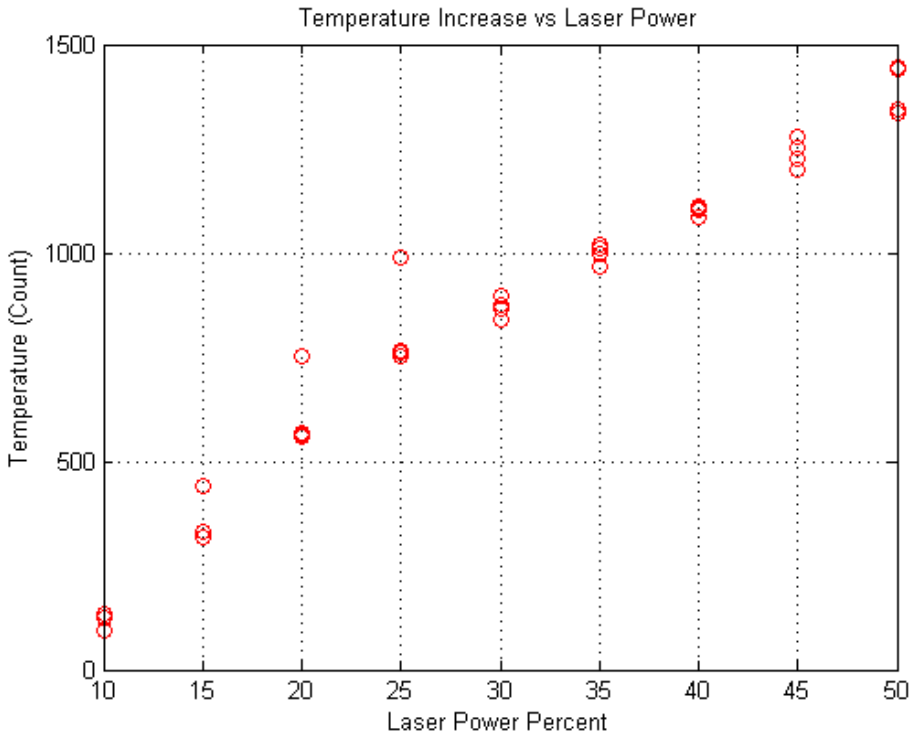

Figure 17: Temperature Increase vs. Laser Power

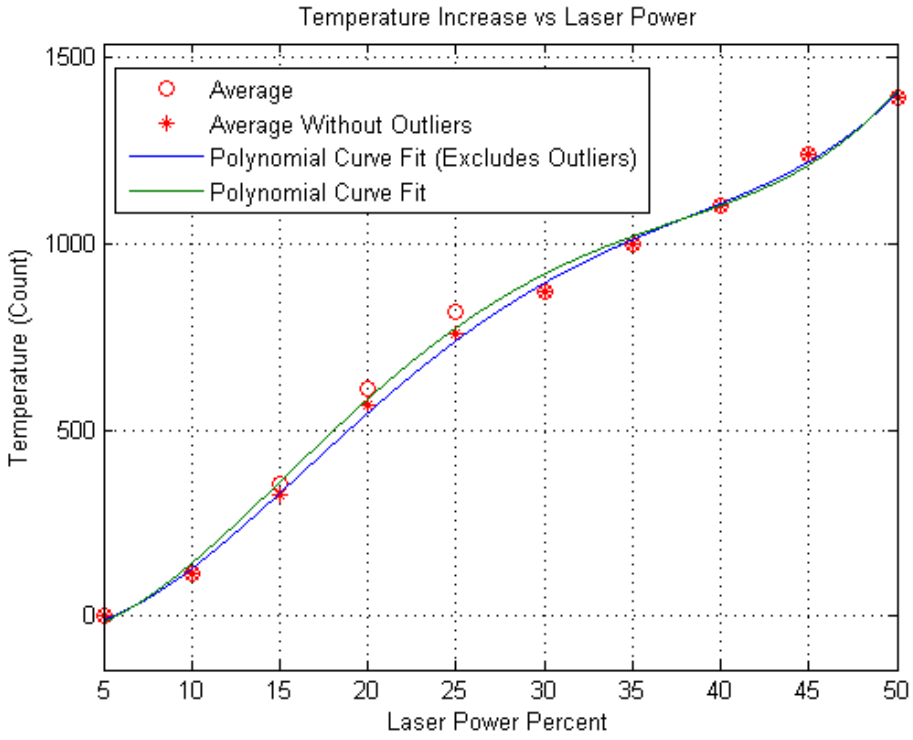

Figure 18: Temperature Increase vs. Laser Power Fit

Single Line Test

The Strategy for sintering a single line is split into three phases. The first phase is to move the galvanometers to the beginning of the scan line. This phase is not critical and no data is recorded. The purpose of this phase is simply to make the calculations in the following phase easier by ensuring only temperature data of the scan line is recorded. The second phase is to scan the camera over the scan line with zero laser power. This gives the original temperature distribution of the scan line, which is fed into the MATLAB program that computes the difference between the pre-sintering temperature and the desired temperature. The program then uses the laser power to temperature increase transfer function to parse the line into subsections that each have a constant, integer value of power and uses that data to create a scan file that is sent to the Cambridge EC1000. The final phase returns the galvanometers to the beginning of the scan line and uses the scan file created in the previous phase to sinter the line using the variable power percentages defined by each subsection.

An example of how a fixed laser power affects the post-sintering temperature is seen in Figure 19. As you can see, the post-sintering temperature mimics the pre-sintering temperature and deviates from the desired temperature. An example result of in-situ laser control is seen in Figure 20. Using a large subsection size, the closed loop laser control scheme will create a sawtooth-like resultant temperature with much less deviation from the desired temperature than an open loop control scheme. As the subsection size decreases, this deviation will also decrease.

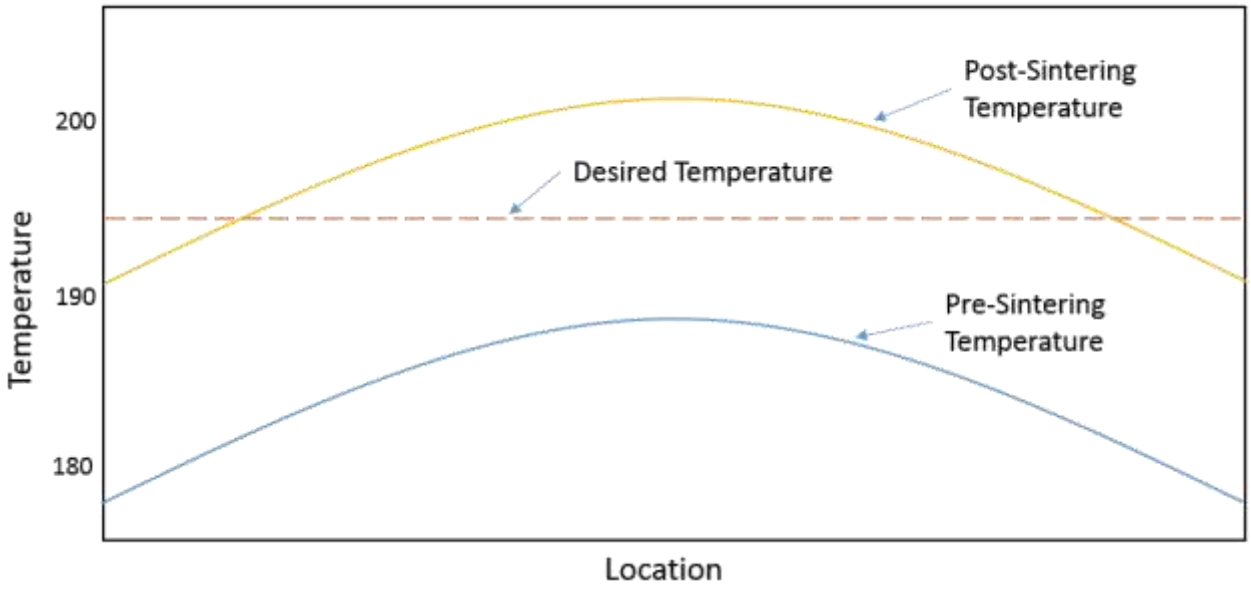

Figure 19: Example Open Loop Laser Result

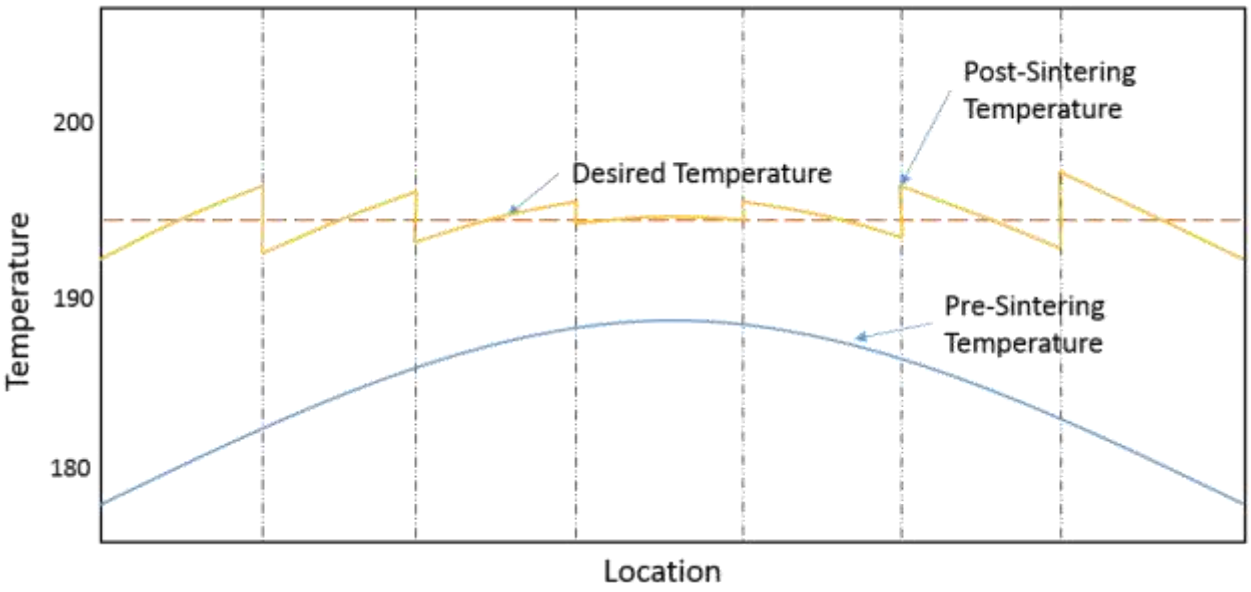

Figure 20: Example Closed Loop Result

Subsection Spacing

In theory, the subsection spacing can be reduced to the length of a single pixel on the MWIR camera, effectively turning the laser into a pulsed source that delivers the exact amount of

energy to raise each voxel of powder to the desired temperature. This will drive the error between the actual and desired post-sintering temperature to zero, but is likely not be the most effective means of in-situ control. There are a number of disadvantages to this method, including increasing the computation time and difficulty. For the high resolution MWIR camera, this method can result in hundreds of thousands of temperatures per layer that need to be analyzed. Another disadvantage is that any amount of error in the laser power control or velocity compensation will be compounded and lead to a poor thermal profile of the build surface.

It was decided that an acceptable tradeoff between computation time and temperature control precision came from limiting the laser power percent to integer values. This creates a dynamic subsection spacing where a new subsection is created once the predicted temperature of the previous subsection reaches a certain limit. An example result of this dynamic subsection method is seen in Figure 21. This method produces a relatively small error between the desired post-sintering temperature and the theoretically obtainable post-sintering temperature, while not adding significant time to the build.

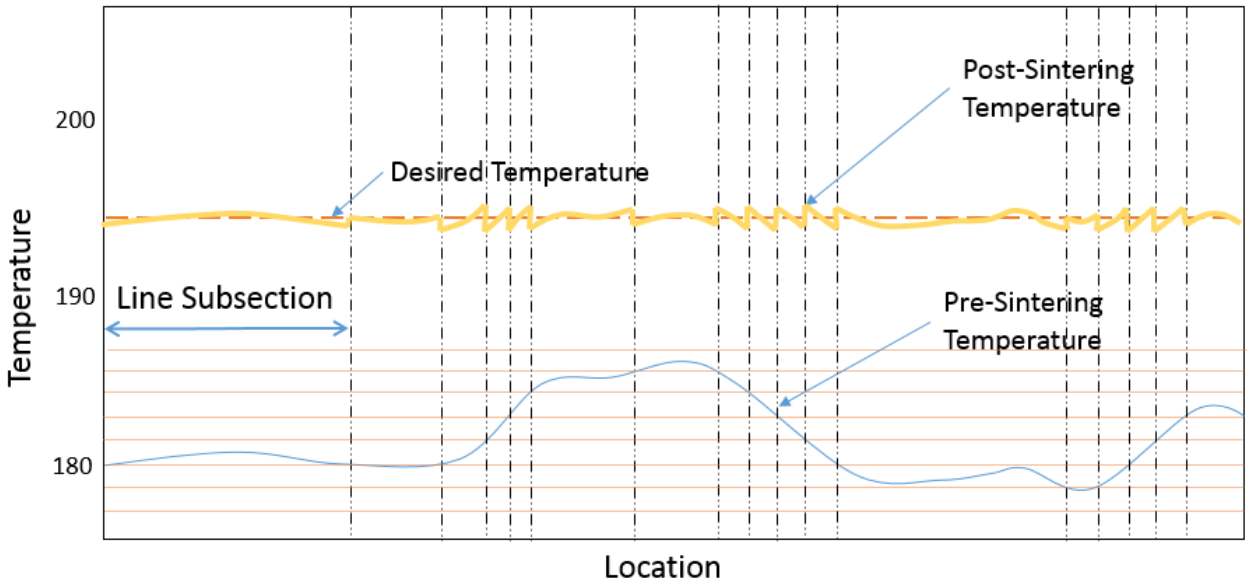

Figure 21: Example Dynamic Sectioning Result

Chapter 5: Results

A total of 13 in-situ laser control trials were run, the majority of which showed vast improvements over the baseline, constant power trials. The number of trials is admittedly on the low side, but the results are encouraging. This section will highlight some characteristic results. Result plots for all completed trials are given in Appendix A.

Baseline

In order to understand the results from the in-situ control, the baseline results must first be analyzed. The following results are from a test run using the same procedure as the in-situ control tests except a fixed laser power was used for the entirety of the scan line. An IR image taken with the boresight MWIR camera is shown in Figure 22. The figure identifies the pixel on the IR camera that the laser is currently firing at (the hottest pixel in view). Despite the galvanometers moving the laser, the laser spot will remain on the same pixel of the IR camera throughout the build due to the laser and MWIR camera co-alignment. The temperature of the pixel corresponding to the laser spot will be used to identify the pre-sintering and post-sintering temperatures for all trials.

The temperature of the laser spot pixel for all 1500 frames during one of the baseline trials is shown in Figure 23. For the first 430 frames the temperature is constant, except for some noise. This is due to the time delay between when the MWIR camera begins recording and the galvanometer begins moving. This time delay will vary from trial to trial. From frames 430 to 490 the galvanometer is moving to the beginning of the scan line. As you can see, the temperature rises during this period due to the temperature gradient in the powder. From frames 490 to 540 the galvanometer is running the laser over the scan line with zero laser power. This step provides data on the initial temperature profile of the scan line. From frames 540 to 600 the galvanometer

is returning to the beginning of the scan line. From frames 600 to 650 the galvanometer is scanning the laser line, now with a fixed, non-zero laser power. A small spike at the beginning of this region is observed due to suboptimal tuning of the velocity compensation. It is observed that the temperature profile during the lasing mimics that of the pre-scan, just at a higher temperature. From frames 650 to the end of the trial, the laser is off and the galvanometers are not moving. The temperature change observed in this region is due to heat radiating and convecting away from the newly sintered region.

Once these regions are identified, the data can be displayed in a more useful manner. Figure 24 shows the same data with the pre-scan and laser scan coinciding. It is much clearer from this image how the post-sintering temperature tracks that of the pre-sintering temperature. This can also be seen in Table 1, which displays the average temperature, the maximum difference of the temperatures and the standard deviations of the temperatures for the pre-sintering and post-sintering temperature on all 3 baseline trials. The table also shows the change in maximum temperature difference and standard deviation from the pre-sintering to post-sintering temperature data. All baseline trials, which can be seen in Appendix A, exhibit a post-sintering temperature profile that is heavily influenced by the pre-sintering profile. This effect can also be clearly seen in Figure 16.

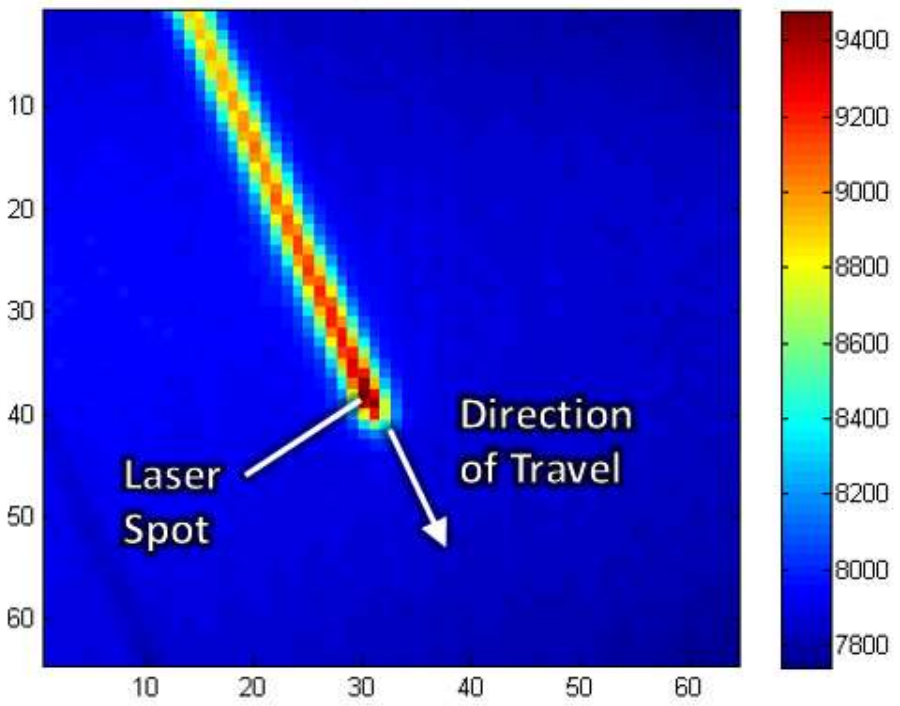

Figure 22: Boresight IR Image

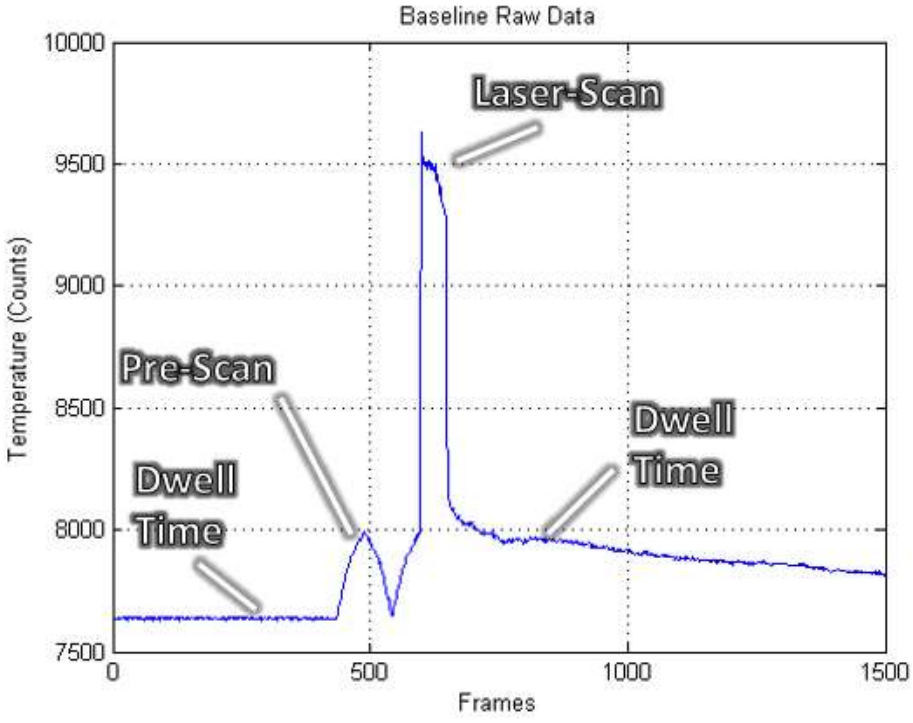

Figure 23: Baseline Raw Temperature Data

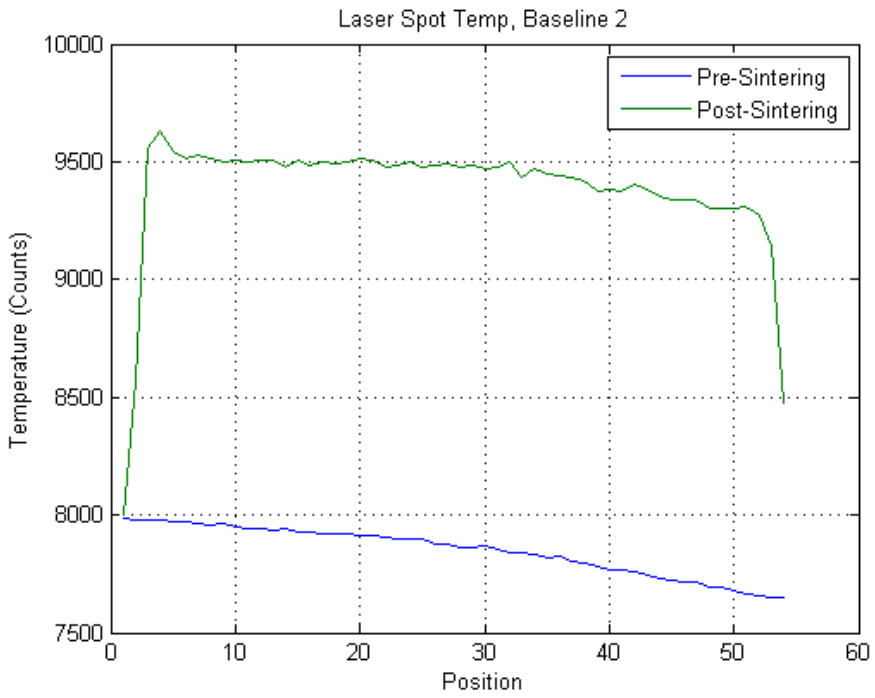

Figure 24: Baseline Temperature Data

Table 1: Baseline Temperature Measurements

Trial	Avg. Pre-Sintering Temp.	Max Pre-Sintering Temp Difference	Pre-Sintering Temp STD	Avg. Post-Sintering Temp	Max Post-Sintering Temp Difference	Post-Sintering Temp STD	Temp Diff Change	Temp STD Change
1	8022.6	291	88.6	9584.1	522	89.5	-79.38%	-1.02%
2	7843.7	314	93.2	9442.4	256	73.2	18.47%	21.46%
3	7751.7	316	97.8	9292.1	414	75.8	-31.01%	22.49%

Powder Insulation

Laser control requires highly specialized sensors that collect data with resolutions not typically available. This allows for examination of complex powder phenomenon, such as determining the extent of heat conduction throughout the top layer of powder. As a product of recording large amounts of thermal data during the scan lines, data was recorded immediately

following the scan line where the galvanometer is stationary. This allows for probing the temperature values for sections of the build surface as the powder cools with high resolution. The cooling temperatures can be seen in Figure 25. The data in this figure was taken immediately following the laser turning off when the galvanometer is stationary. The blue line is the temperature recorded at the pixel corresponding to the center of the laser spot and the green line is the nearest pixel that was outside the laser spot, a mere 3 pixels (approximately 2.5 mm) away from the center of the laser. As you can see, over the 0.25 seconds recorded, the laser spot pixel cooled rapidly while the adjacent point's temperature was unchanged. This supports the view that the nylon material is highly insulating and shows that radiation and convection to the build chamber are the primary modes of heat transfer on the surface of the powder and they drastically outweigh the effect of conduction.

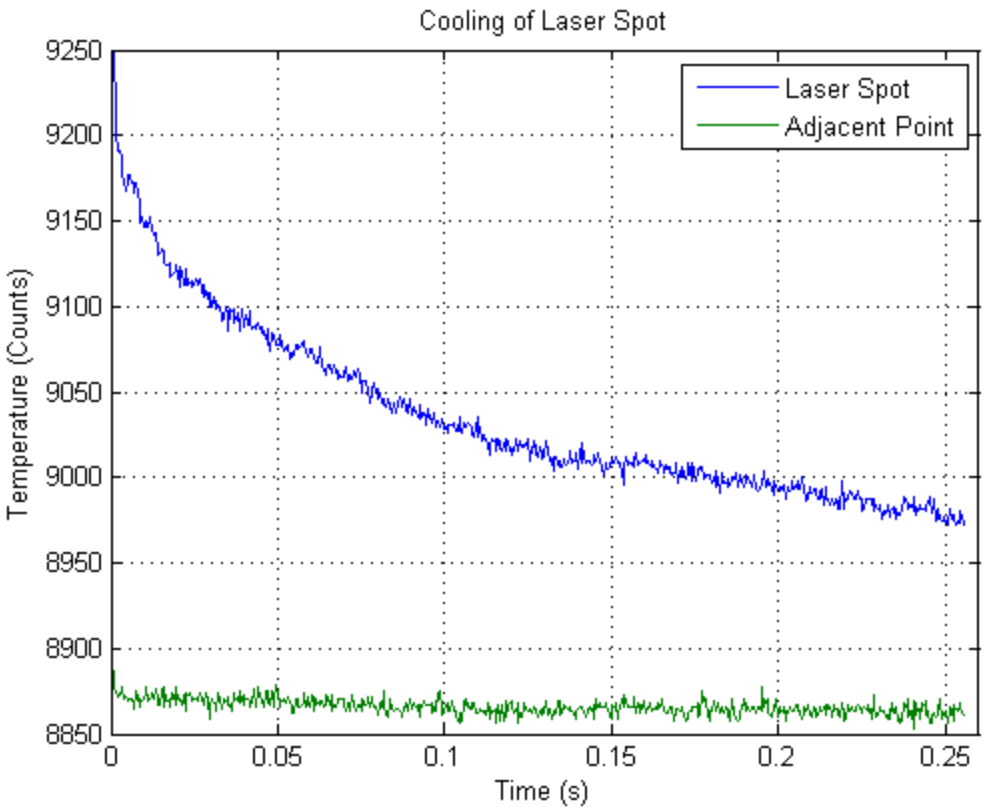

Figure 25: Cooling of Laser Spot

In-Situ Control

In-Situ control of the laser power was performed as specified in the methods chapter. The pre-sintering temperature profile for one of the trials is seen in Figure 26. The first subplot shows the raw temperature data from the pre-scan with the first 340 and the last 1100 frames being dwell time for the galvanometer. The second subplot shows a close-up of the non-dwell time region which is the temperature profile of the scan line. This temperature is fed through the laser power to temperature increase transfer function with a desired post-sintering temperature of 9000 Counts. The resulting laser power profile is seen in Figure 27. The galvanometer coordinates for the scan line are 11 – 46. As you can see, the scan line was split into 13 subsections, each with its own length and laser power percentage based on the pre-sintering temperature profile.

The raw result of this in-situ laser control trial is shown in Figure 28. This data is read the same way as the raw data for the baseline trials, where the beginning and ending of the data is galvanometer dwell time, the first hump is traversing over the scan line backwards then forwards with no laser power, and the second hump is traversing over the scan backwards then forwards with the variable laser power defined in Figure 27. Figure 29 displays the same data with the dwell times removed and the pre-sintering temperature and post-sintering temperature coinciding. The red line is the same as the line in Figure 26, the pre-sintering temperature that is used to determine the subsection laser power percentages. The blue line is data from the same location as the red line, but roughly two minutes later. The process to analyze the pre-sintering temperature, create a scan file, and implement the laser control took roughly 2 minutes. The blue line was taken as the first step of the in-situ control scan file and is used to determine the extent to which the system has changed in the 2 minutes since the initial data was taken. If the blue line is significantly different than the red line, it is expected that the in-situ control will not perform as expected, as the control is based off an inaccurate representation of the system at the time it is implemented. The green line is the post-sintering temperature. It is observed that this temperature is centered on the desired temperature of 9000 Counts and is not influenced by the pre-sintering temperature gradient. The black line is the result of the delivered laser power defined in Figure 27 fed back through the laser power to temperature increase transfer function to get an expected temperature increase. This number is added to the blue line, the actual pre-sintering temperature. If the in-situ control strategy is working correctly, this line should match closely with the green line, the actual post-sintering temperature. Note that the black line is not a straight line exactly at the desired temperature because it was fed twice through the transfer function that rounded the delivered power to integer values.

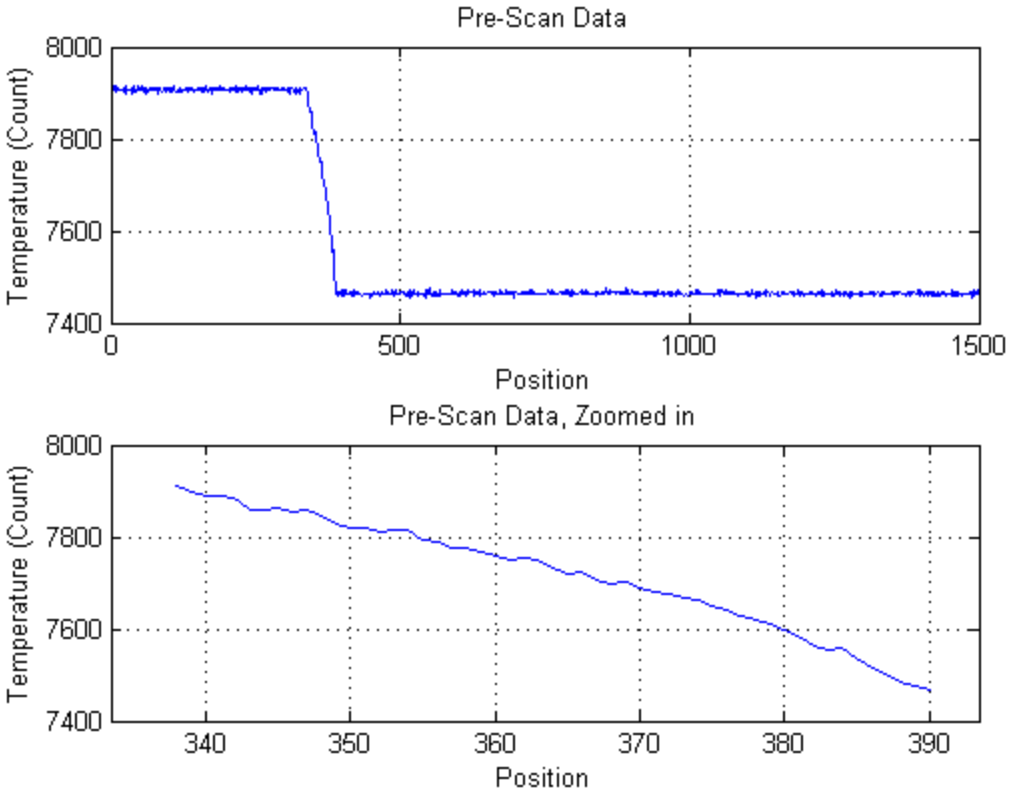

Figure 26: Pre-Sintering Temperature Profile

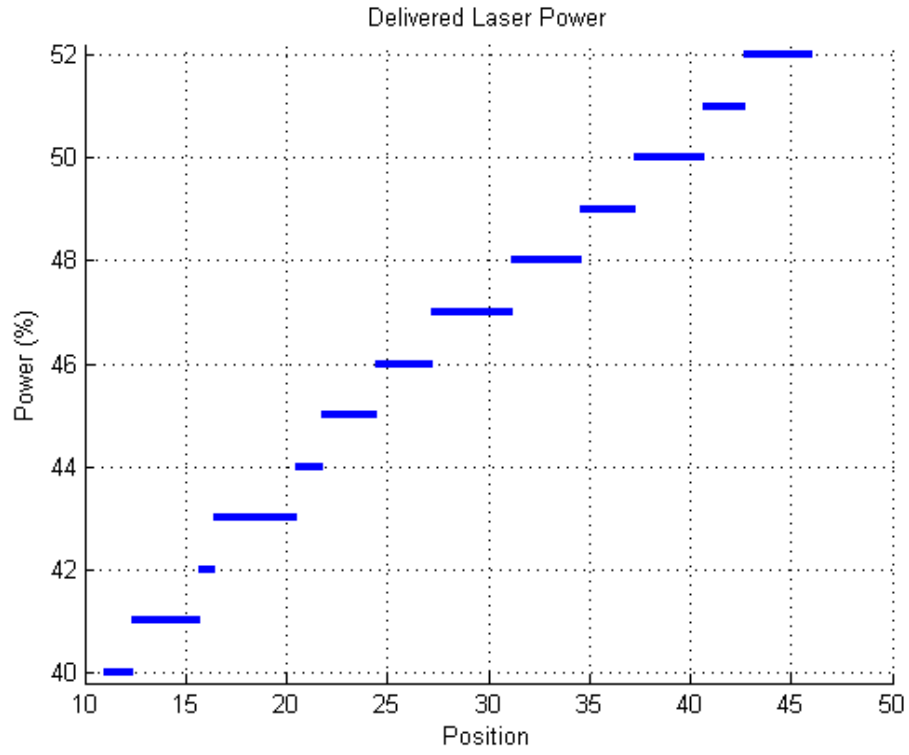

Figure 27: Delivered Laser Power

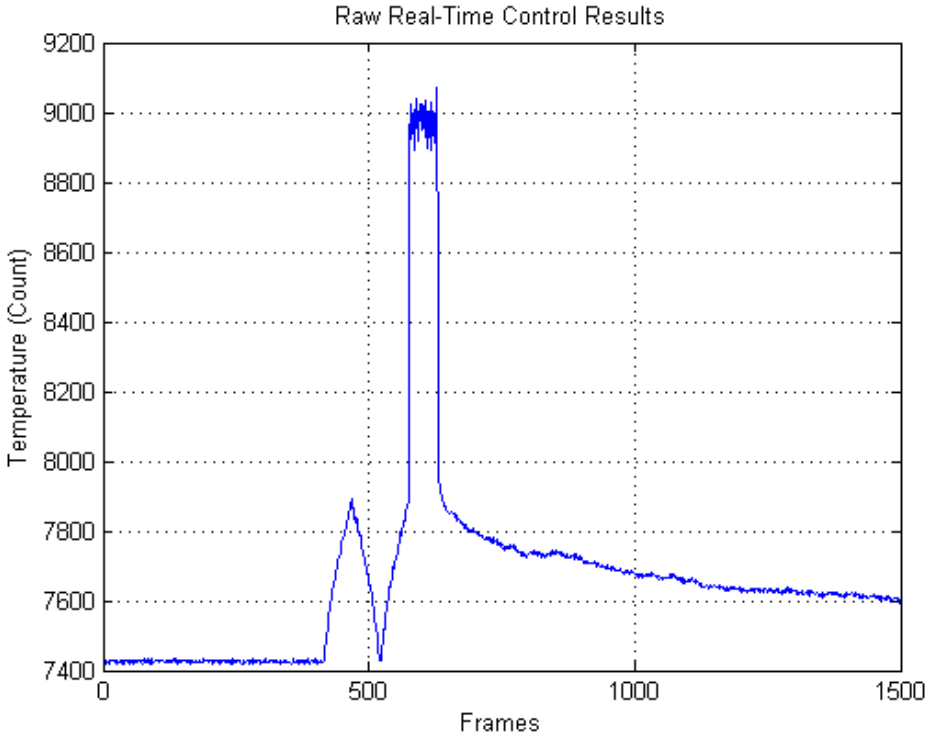

Figure 28: Raw In-Situ Laser Control Results

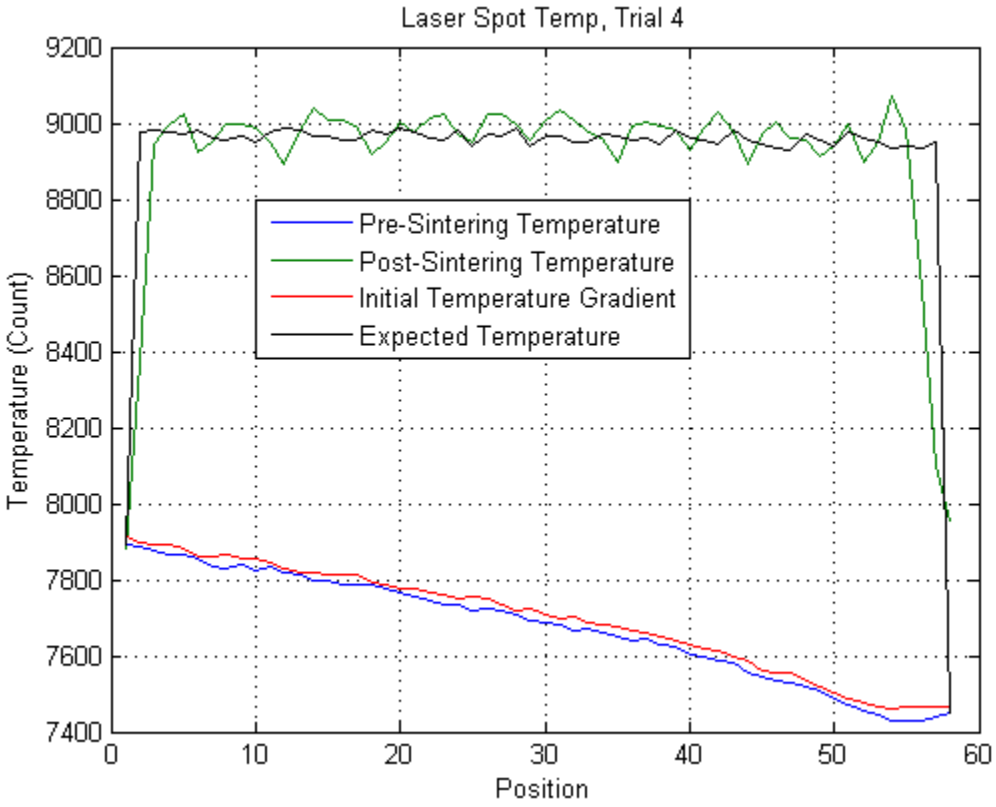

Figure 29: In-Situ Laser Control results for Trial 4

This trial performed exceptionally well and showed that a high level of laser control is possible with the method proposed. The results of all in-situ control trials are displayed in Table 2 as well as Appendix A. As can be seen from the "Temp Diff Change" and the "Temp STD Change" columns of Table 2, all of the trials exhibited a post-sintering temperature profile that was superior to the pre-sintering temperature in terms of uniformity. This cannot be said of the baseline trials, whose post-sintering temperature profile mimicked the pre-sintering profile. This result indicates that the in-situ control experiments were successful and the proposed control method is valid.

It should be noted that the data is missing for trials 3, 8, and 13. This is due to errors in the implementation of control for those trials, not from flaws in the control method. On trial 3, the scan file was corrupt and caused the laser to double scan a subsection of the line, resulting in a large temperature spike. This occurred because of a bug in the MATLAB file used for creating the scan files. During trial 8, the boresighted MWIR camera was shifted slightly prior to the initial pre-sintering temperature profile being recorded. This caused the pixel corresponding to the laser spot to shift and the power percentages being calculated off the incorrect spots on the powder surface. The result was a line whose power was not determined by its own initial thermal profile, but from an adjacent line. Trial 13 is believed to have been successful, but the data was not recorded successfully by the MWIR camera. The recording of the MWIR camera is triggered off the initialization command from the EC1000 at the start of sintering. The MWIR camera software reliable responds quickly to this trigger and begins recording immediately, but the EC1000 and galvanometer have a time delay. During this trial, the delay exceeded the time it took for the camera to record the predetermined 1500 frames (approximately 670 milliseconds) and, thus, the post-sintering temperature was not recorded.

The data in Table 2 shows that all in-situ control trials outperformed the baseline temperature gradient, yet to a varying extent. One example of a trial that did not perform as well as predicted is seen in Figure 30. This trial exhibits overcompensation of the laser power and the temperature grows over the length of the line. This clearly does not agree with the expected post-sintering temperature and it is unclear exactly why at this point. What is known is that this test was performed at the lowest laser power. It is possible that the laser power to temperature increase transfer function was inaccurate in this power range or the lower power used otherwise affected the result of this trial. Another example of a trial that was not exceptional is seen in Figure 31.

This trial exhibits slight under compensation of the laser power, due to a limit placed on the maximum laser power. This scan line started at 50% power then increased to 55% power throughout the length of the line. The laser power to temperature increase transfer function used to determine these powers was built from empirical data of tests up to 50% power. The transfer function was limited to a maximum power output of 55%, as exceeding the tested powers by too much was undesirable as it was unclear how the temperature would react in that region. This means that the entirety of this line used laser powers outside the tested power region and was capped at 55%, causing the sharper decrease in temperature in the latter third of the line. This transfer function limit is likely the cause of the poorer results from this trial. Trials 8, 9, 10, and 11 all reached the laser power cap and have a corresponding temperature drop throughout the line. Figures of all the laser spot temperature for all trials are given in Appendix A.

Table 2: In-Situ Control Temperature Measurements

Trial	Avg. Pre-Sintering Temp.	Max Pre-Sintering Temp Difference	Pre-Sintering Temp STD	Avg. Post-Sintering Temp	Max Post-Sintering Temp Difference	Post-Sintering Temp STD	Temp Diff Change	Temp STD Change
1	762	457	142.2	8482.8	389	89.28	14.88%	37.22%
2	762.2	402	126	9083.6	210	41.91	47.76%	66.74%
3	--	--	--	--	--	--	--	--
4	7682.4	439	124.5	8978.1	183	40.8	58.31%	67.23%
5	8018.4	326	96.6	8901.6	149	31.5802	54.29%	67.31%
6	7768.9	377	114.6	9042.1	245	68.4	35.01%	40.31%
7	7677.3	374	110.2	9292.4	250	52.9	33.16%	52.00%
8	--	--	--	--	--	--	--	--
9	7663.7	396	112.2	8953.3	191	45.3	51.77%	59.63%
10	7610.4	385	114.8	8988.2	258	60.9	32.99%	46.95%
11	7575.1	391	116.4	8931.2	303	79.8	22.51%	31.44%
12	7745	355	103	8761	124	24.2	65.07%	76.50%
13	--	--	--	--	--	--	--	--

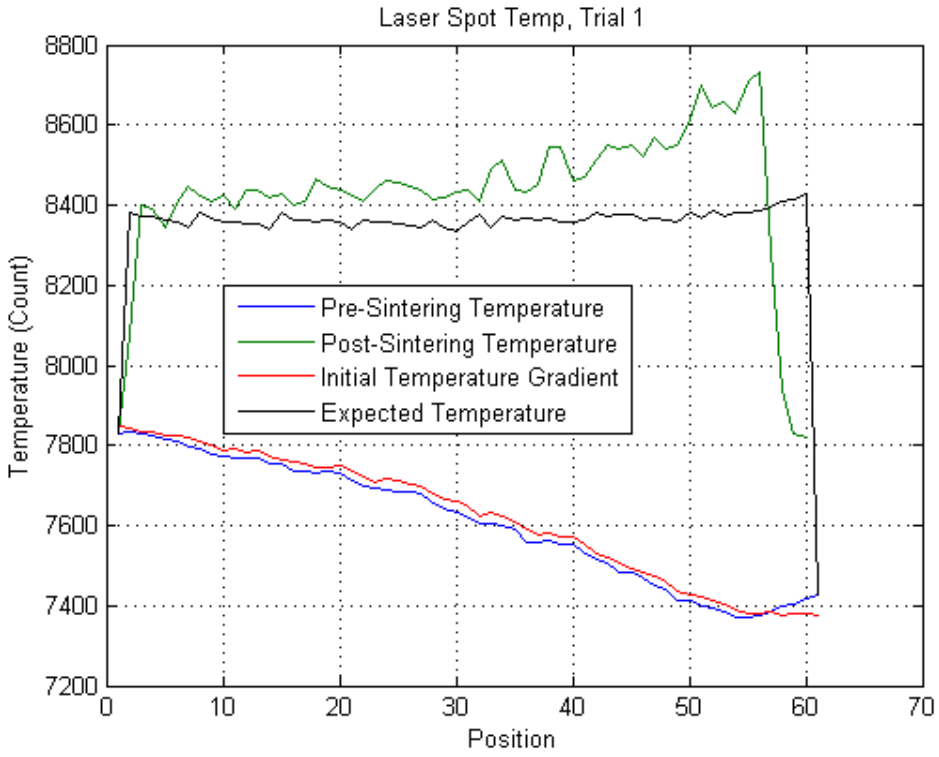

Figure 30: Laser Power Overcompensation

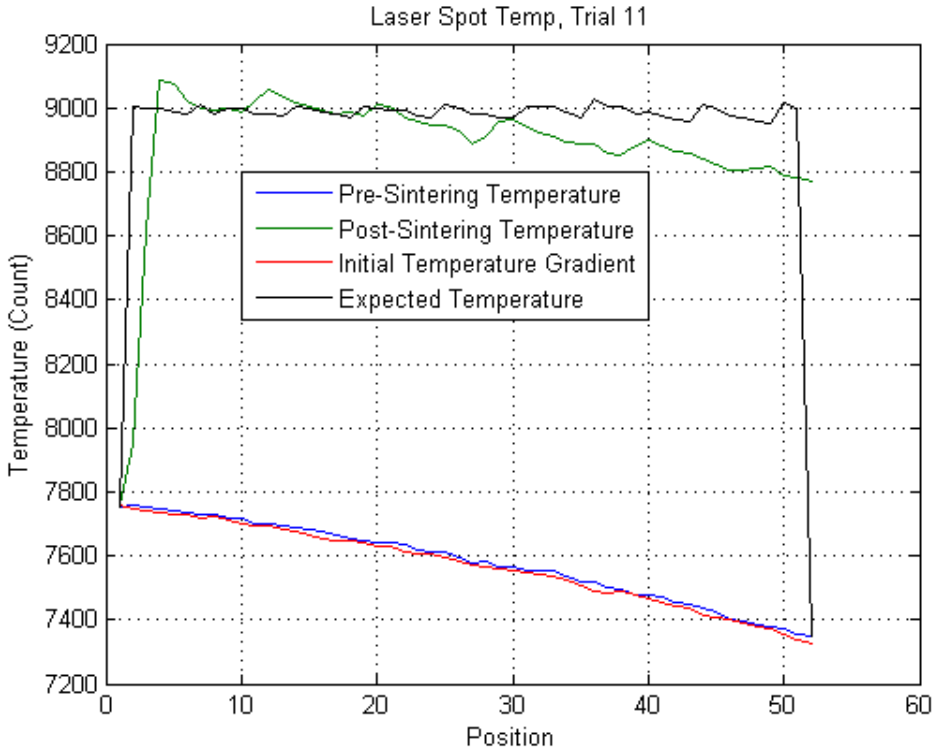

Figure 31: Laser Power Limit

Chapter 6: Conclusion

This thesis presents a method of in-situ laser control for SLS and details the results of testing said control method. The hypothesis that the traditional, fixed laser power method of sintering would uniformly increase the temperature of the powder and preserve its initial temperature gradient was confirmed. This revealed the need for an improved control method where the initial powder bed temperature profile could be diminished. The method proposed is to measure the powder surface with a MWIR sensor, determine the difference between the current temperature and the desired temperature, then regulate the laser energy deposition in order to counteract the thermal profile and achieve a uniform post-sintering temperature.

The results of testing are overwhelmingly positive, with each test outperforming the baseline control method. Temperature variations throughout a scan line were shown to greatly diminish using the in-situ control method employed. The effect of the pre-sintering thermal profile on the post-sintering temperature was reduced up to 65%. While not every trial performed exceptionally well, all showed improvement over the baseline. This increased control over laser energy deposition and the corresponding decrease in post-sintering temperature gradients is advantageous for creating high-quality components via Selective Laser Sintering. By decreasing the thermal gradient in the post-sintering part, the mechanical and dimensional properties of the part will be improved (Rajan & Wood, 2001).

The next step is to take this method and expand it to an entire build. Using the same strategy, multiple scan lines can be controlled and stitched together to form cross-sections of the component whose temperature uniformity is much greater than if the traditional, fixed power control method was used. Another avenue of further exploration is using a faster control system

for real-time laser control. This will likely include additional hardware and software that is capable of varying the laser power in real-time without the need to split up the scan line into subsections.

Appendix A: In-Situ Laser Control Results

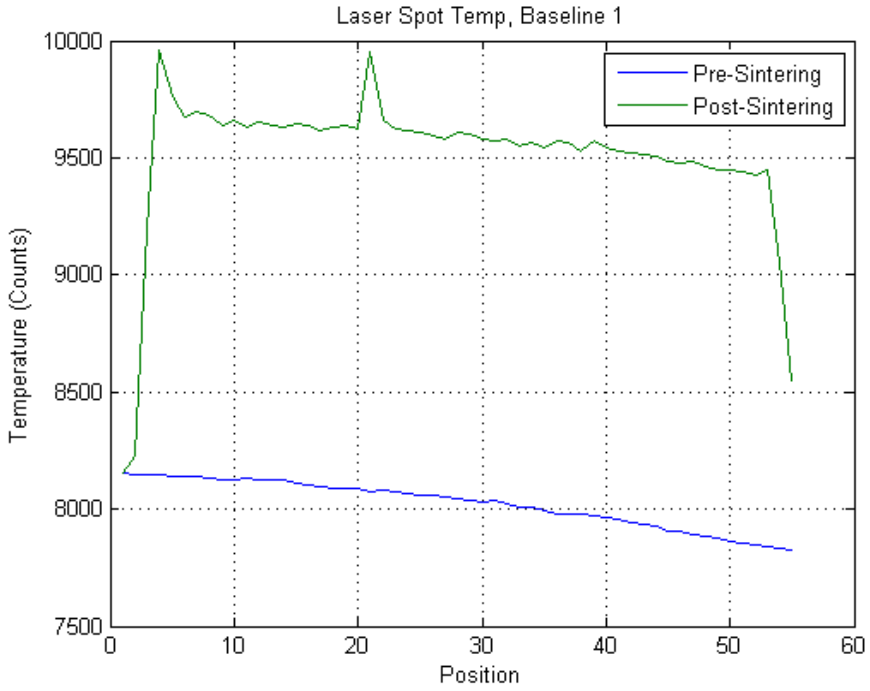

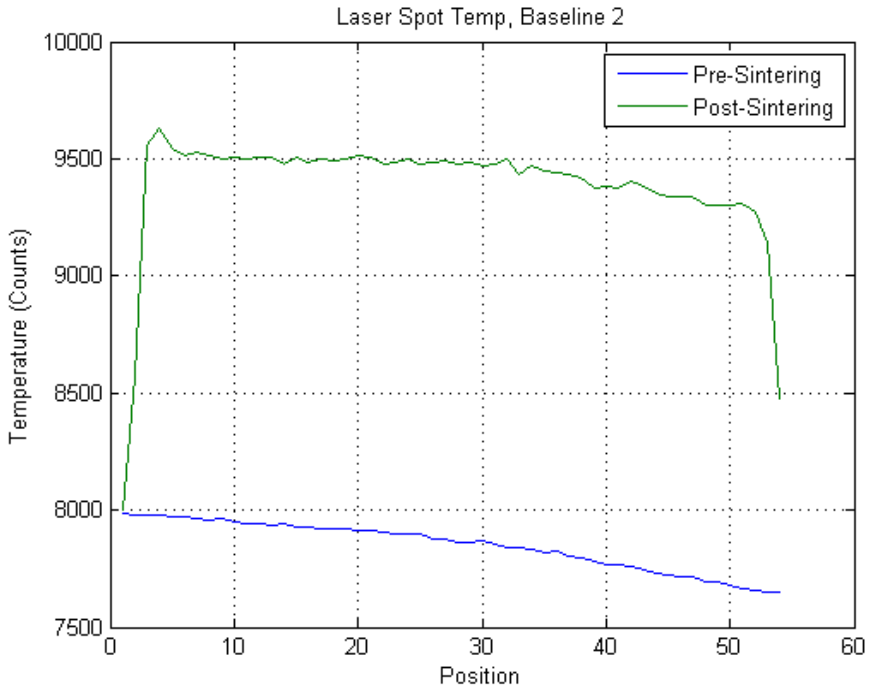

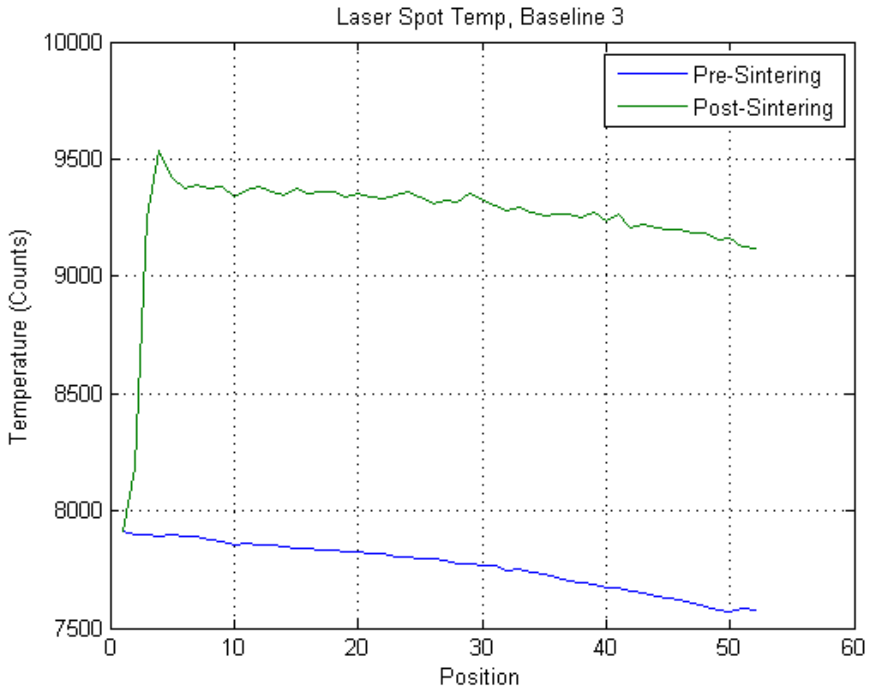
Laser Spot Temp, Baseline 3
Pre-Sintering
Post-Sintering
Temperature (Counts)
Position
10000
9500
9000
8500
8000
7500
0
10
20
30
40
50
60

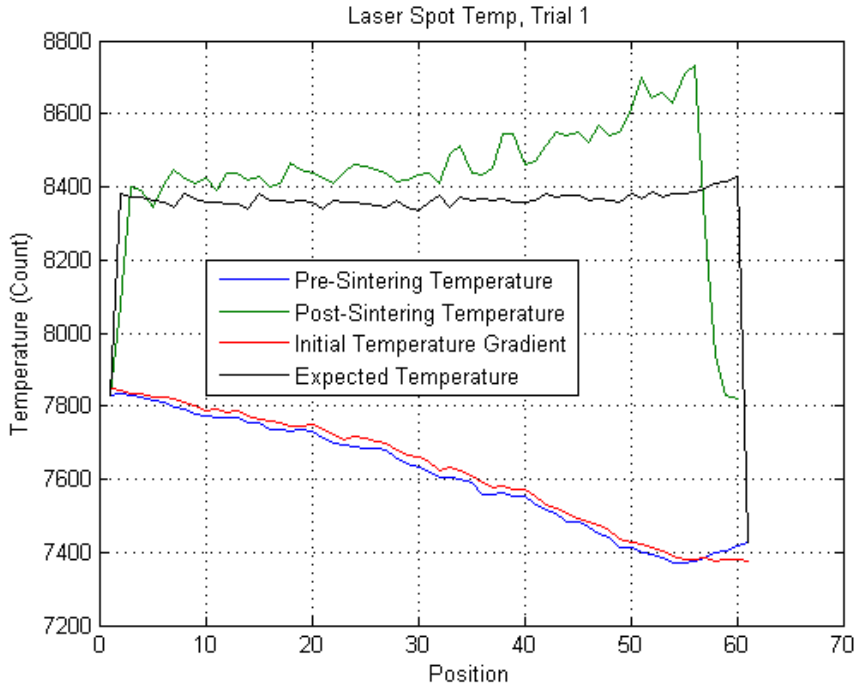
Laser Spot Temp, Trial 1
Pre-Sintering Temperature
Post-Sintering Temperature
Initial Temperature Gradient
Expected Temperature
Temperature (Count)
Position
8800
8600
8400
8200
8000
7800
7600
7400
7200
0
10
20
30
40
50
60
70

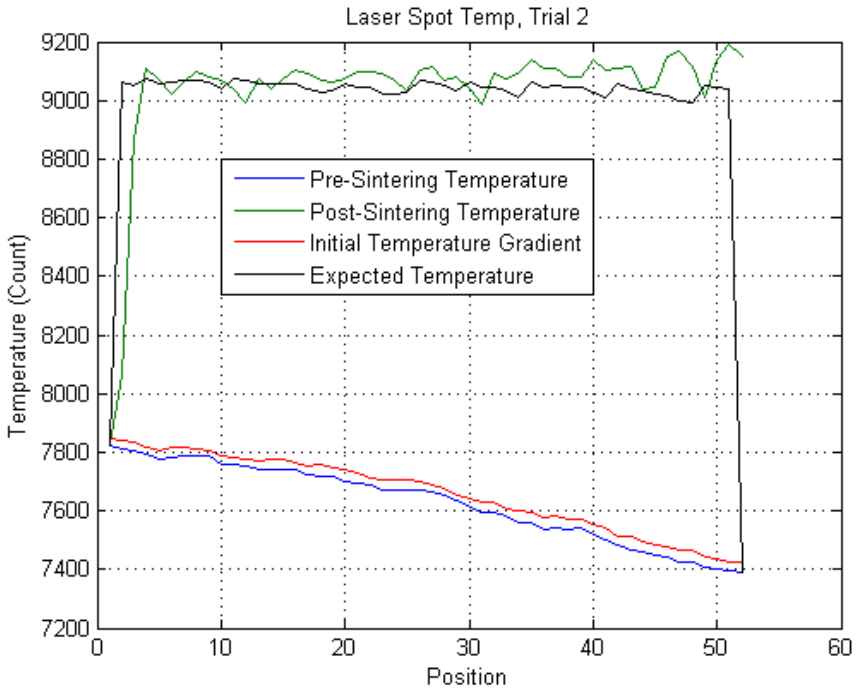
Laser Spot Temp, Trial 2
Temperature (Count)
Position
Pre-Sintering Temperature
Post-Sintering Temperature
Initial Temperature Gradient
Expected Temperature
9200
9000
8800
8600
8400
8200
8000
7800
7600
7400
7200
0
10
20
30
40
50
60

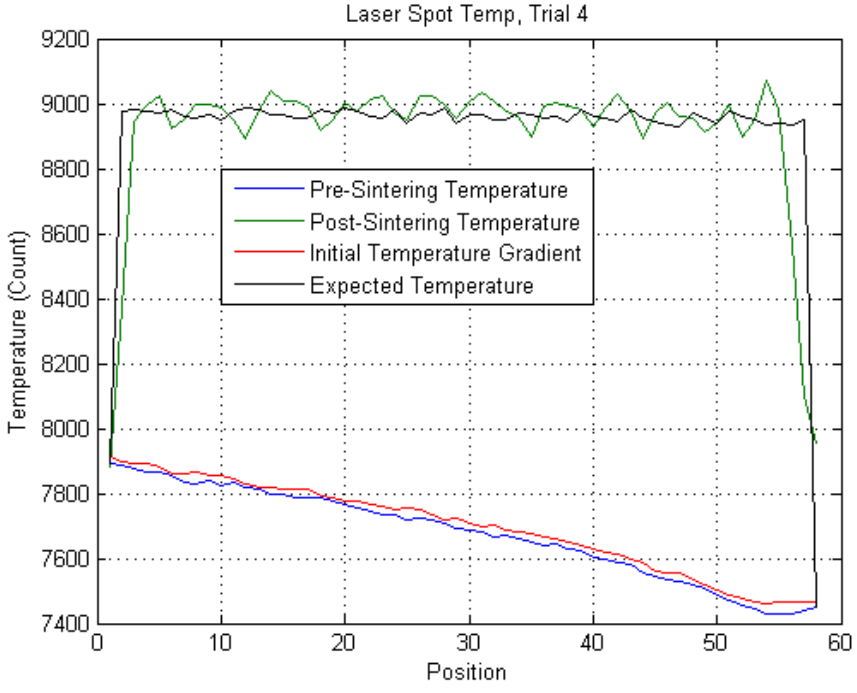
Laser Spot Temp, Trial 4
Temperature (Count)
Position
Pre-Sintering Temperature
Post-Sintering Temperature
Initial Temperature Gradient
Expected Temperature
9200
9000
8800
8600
8400
8200
8000
7800
7600
7400
0
10
20
30
40
50
60

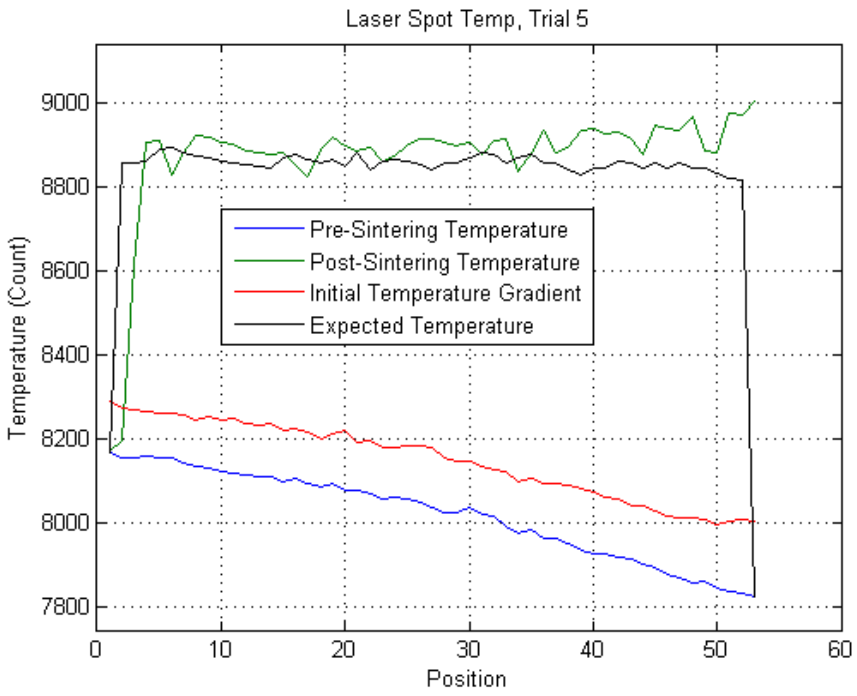
Laser Spot Temp, Trial 5
Temperature (Count)
Position
Pre-Sintering Temperature
Post-Sintering Temperature
Initial Temperature Gradient
Expected Temperature
9000
8800
8600
8400
8200
8000
7800
0
10
20
30
40
50
60

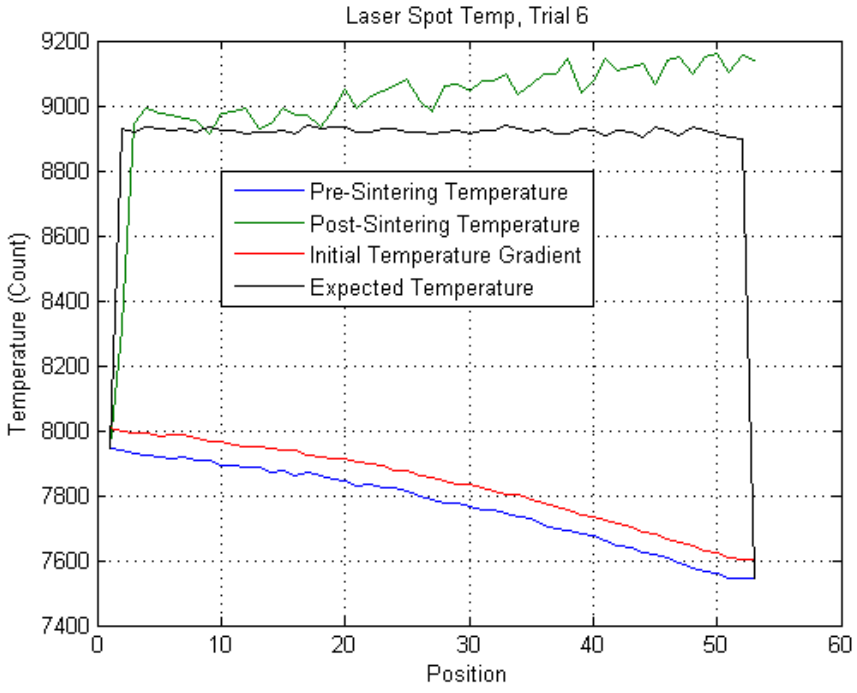
Laser Spot Temp, Trial 6
Temperature (Count)
Position
Pre-Sintering Temperature
Post-Sintering Temperature
Initial Temperature Gradient
Expected Temperature
9200
9000
8800
8600
8400
8200
8000
7800
7600
7400
0
10
20
30
40
50
60

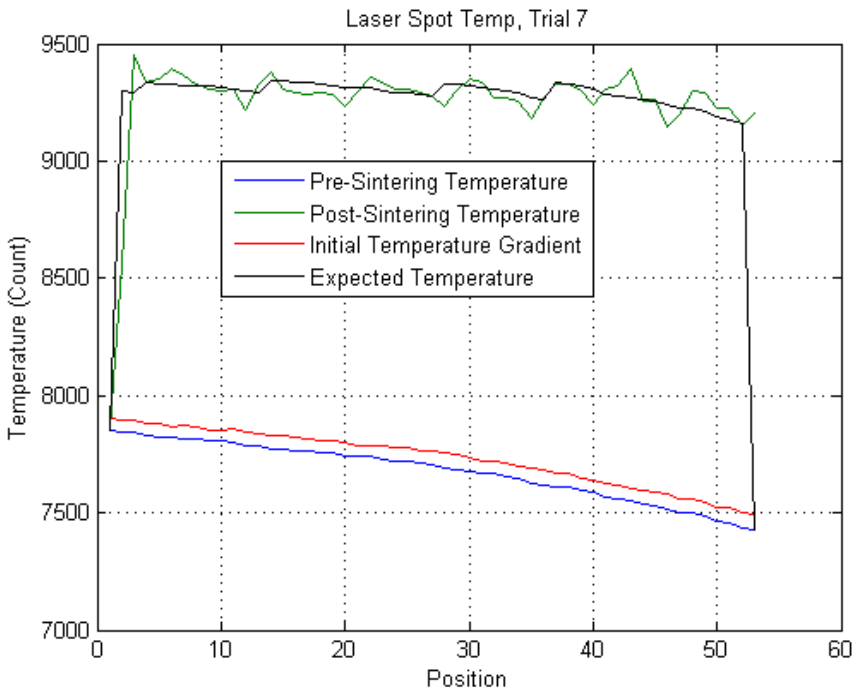
Laser Spot Temp, Trial 7
Temperature (Count)
Position
Pre-Sintering Temperature
Post-Sintering Temperature
Initial Temperature Gradient
Expected Temperature
9500
9000
8500
8000
7500
7000
0
10
20
30
40
50
60

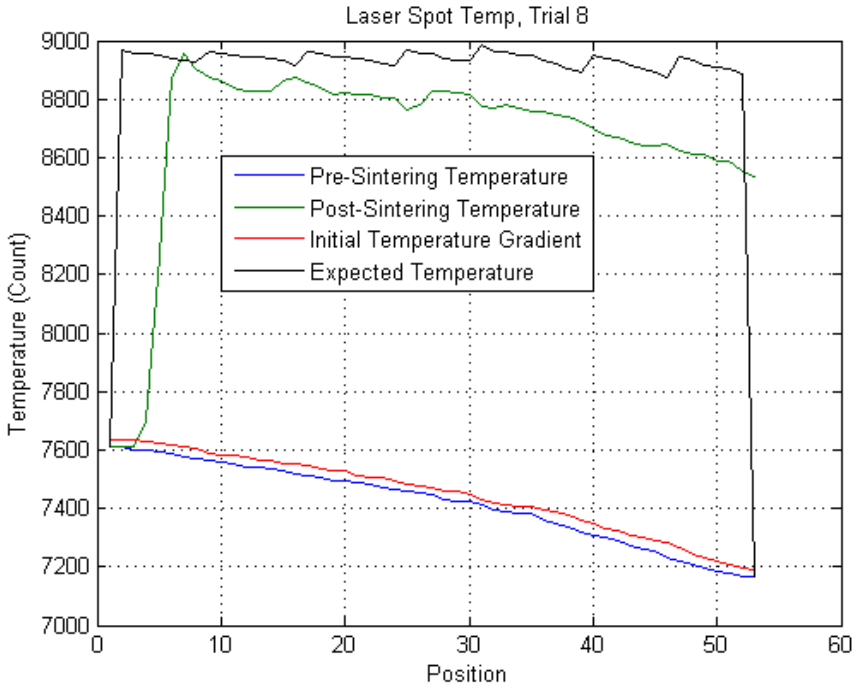
Laser Spot Temp, Trial 8
Temperature (Count)
Position
Pre-Sintering Temperature
Post-Sintering Temperature
Initial Temperature Gradient
Expected Temperature
9000
8800
8600
8400
8200
8000
7800
7600
7400
7200
7000
0
10
20
30
40
50
60

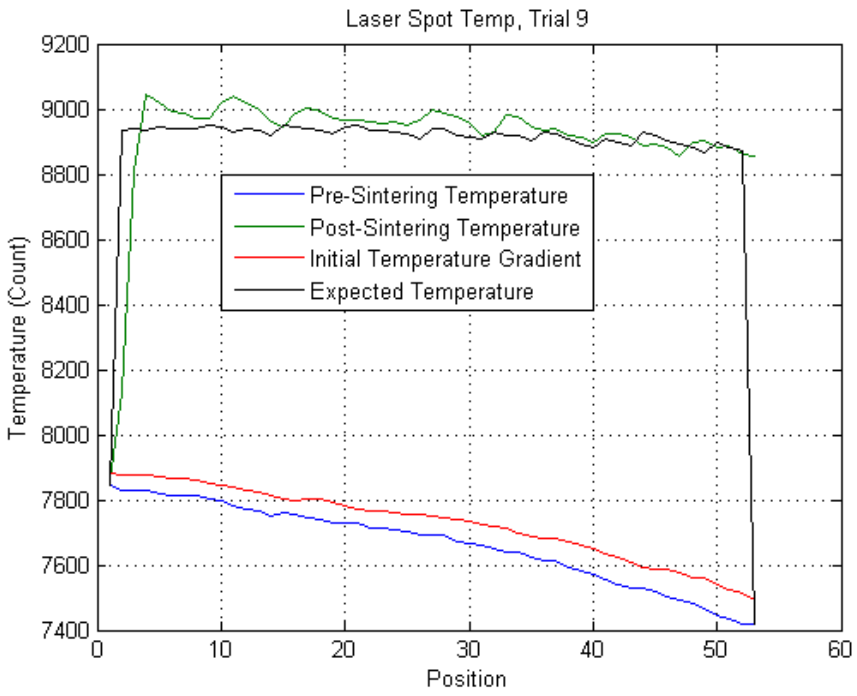
Laser Spot Temp, Trial 9
Pre-Sintering Temperature
Post-Sintering Temperature
Initial Temperature Gradient
Expected Temperature
Temperature (Count)
Position
9200
9000
8800
8600
8400
8200
8000
7800
7600
7400
0
10
20
30
40
50
60

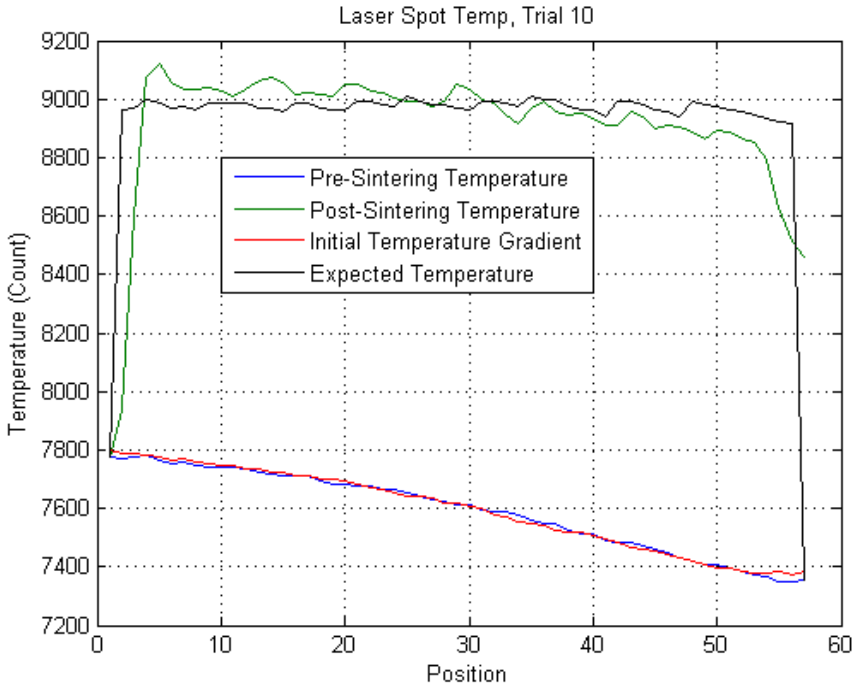
Laser Spot Temp, Trial 10
Pre-Sintering Temperature
Post-Sintering Temperature
Initial Temperature Gradient
Expected Temperature
Temperature (Count)
Position
9200
9000
8800
8600
8400
8200
8000
7800
7600
7400
7200
0
10
20
30
40
50
60

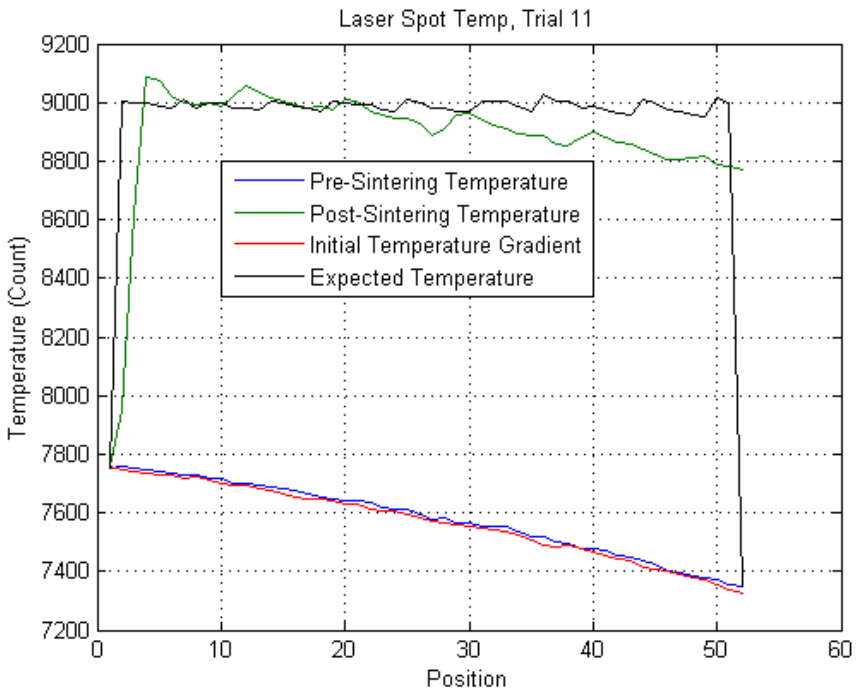
Laser Spot Temp, Trial 11
Temperature (Count)
Position
Pre-Sintering Temperature
Post-Sintering Temperature
Initial Temperature Gradient
Expected Temperature
9200
9000
8800
8600
8400
8200
8000
7800
7600
7400
7200
0
10
20
30
40
50
60

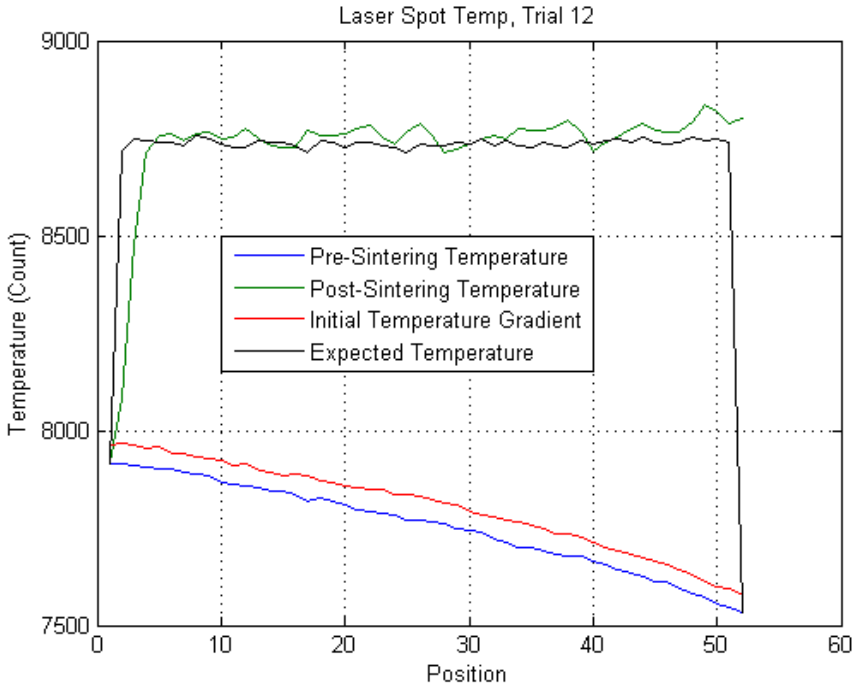
Laser Spot Temp, Trial 12
Temperature (Count)
Position
Pre-Sintering Temperature
Post-Sintering Temperature
Initial Temperature Gradient
Expected Temperature
9000
8500
8000
7500
0
10
20
30
40
50
60

References

Akhloufi, M. A. (2013). Electromagnetic spectrum showing the visible and infrared wavelength intervals. *SPIE.*

Benda, J. A. (1994). Temperature-Controlled Selective Laser Sintering. *Solid Freeform Fabrication Symposium.* Austin.

Bourell, D. L., Watt, T. J., Leigh, D. K., & Fulcher, B. (2014). Performance Limitations in Polymer Laser Sintering. *Physics Procedia*, 147-156.

Carpenter, D. (2014). *Robotics Projects at NAIT*. Retrieved from http://www.acamp.ca/.

Hall, P. (2015). SLS Process Overview. (T. Phillips, Interviewer)

Koretsky, G. M., Nicoll, J. F., & Taylor, M. S. (2013). *A Tutorial on Electro-Optical/Infrared (EO/IR) Theory and Systems.* Institute for Defense Analyses.

Kruth, J. P., Levy, G., Schindel, R., Craeghs, T., & Yasa, E. (2008). Consolidation of Polymer Powders by Selective Laser Sintering.

Lou, A. a. (2012, December 6). *Selective Laser Sintering, Birth of an Industry*. Retrieved from http://www.me.utexas.edu/news/news/selective-laser-sintering-birth-of-an-industry.

Nelson, J. C., & Barlow, J. W. (1992). *Relating Operating Parameters between SLS Machines which have.* University of Texas at Austin.

Rajan, J. R., & Wood, K. L. (2001). *Experimental Study of Selective Laser Sintering of Parmax.* The University of Texas at Austin.

Scanning patterns in SLM. (2015, 1 30). Retrieved from http://www.insidemetaladditivemanufacturing.com/.

Wroe, W. W. (2015). *Improvements and Effects of Thermal History on Mechanical Properties for Polymer Selective Laser Sintering (SLS).* Austin: University of Texas, Austin.

Zinc Selenide (ZnSe) Windows. (2016, 4 7). Retrieved from Edmund Optics.